

p- 3536



# Autonomous Hybrid Renewable Energy System for Smart Grid Application



**A Project Report**

*Submitted by*

**J.VASANTHAKUMAR - 0920105015**

*in partial fulfillment for the award of the degree*

of

**Master of Engineering**

in

**Power Electronics and Drives**

**DEPARTMENT OF ELECTRICAL & ELECTRONICS  
ENGINEERING**

**KUMARAGURU COLLEGE OF TECHNOLOGY  
COIMBATORE – 641 049**

(An Autonomous Institution Affiliated to Anna University of Technology, Coimbatore)

**ANNA UNIVERSITY OF TECHNOLOGY: COIMBATORE**

**APRIL 2011**

# ANNA UNIVERSITY OF TECHNOLOGY:COIMBATORE

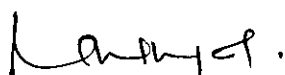
## BONAFIDE CERTIFICATE

Certified that this project report entitled “Autonomous Hybrid Renewable System for Smart Grid Application” is the bonafide work of

J. Vasanthakumar


Register No.0920105015

Who carried out the project work under my Supervision



Signature of the Head of the Department

Dr.Rani Thottungal

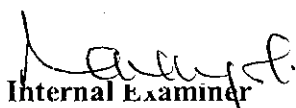


Signature of the Supervisor

Mrs.V.Sharmila Deve

Asst.Proffessor

Certified that the candidate with university Register No. 0920105015 was examined in project viva voce Examination held on 27-4-11



Internal Examiner



External Examiner

DEPARTMENT OF ELECTRICAL & ELECTRONICS ENGINEERING

KUMARAGURU COLLEGE OF TECHNOLOGY, COIMBATORE 641 049

(An Autonomous Institution Affiliated to Anna University of Technology, Coimbatore)

## ABSTRACT

Hybrid Wind and Solar generation shows higher availability of energy. This Project shows Autonomous Hybrid Renewable energy System for Smart grid application.

This project proposed a simulation of hybrid PV-Wind generator and battery system. The PV generator, Wind generator and battery are connected to the different loads through DC bus bar and inverter. The PV generator, wind generator are modeled, MPPT algorithm for Solar and Wind are simulated using MATLAB SIMULINK. The control strategy with PV, Wind generator and battery is proposed to meet the power demand efficiently.

This project presents a simulation of autonomous system for a hybrid PV-wind generator system connected to the DC bus. The dc voltage is inverted and used for loads .An Optimum dispatch controller are proposed to meet the power demand. If power generation of PV and Wind is greater than load, the surplus power stored in battery. If power generation of PV and Wind less than the load, remaining power taken from battery. Suppose the battery at low charging state, it cannot supplies the power, due to that battery is tripped, and also load is tripped. The simulation process illustrated the voltages in the different components of the system with one input conditions of solar radiation, wind speed and temperature. By using renewable energy sources the power demand is compensated and environmental is clean by lower usage of fossil fuels

# CONTENTS

TITLE	PAGE NO
ABSTRACT	i
LIST OF FIGURES	vi
LIST OF TABLES	viii
ABBREVIATIONS	ix
<b>1. INTRODUCTION</b>	
1.1 Introduction of Hybrid Renewable System	2
1.2 Objectives of project	3
1.3 Organization of the thesis	3
<b>2. SMART GRID</b>	
2.1 Introduction of Smart grid	5
2.2 Components of a Smart grid	7
2.2.1 Demand Management	7
2.2.2 Distributed Electricity Generation	9
2.2.3 Transmission and Distribution of grid Management	9
<b>3. COMPONENTS AND MODELING OF HYBRID SYSTEM</b>	
3.1 Block Diagram of Hybrid Renewable System	12
3.2 Modeling of Solar Cell	14

3.2.1	Ideal photovoltaic cell	14
3.2.2	Modeling of the photovoltaic array	14
3.3	Modeling of Wind Energy	18
3.3.1	Mechanical power extraction from the wind	18
3.3.2	Rotor power characteristics	21
3.3.3	Permanent magnet synchronous generator model	22
3.4	Modeling of Lead-Acid battery	23
3.4.1	Lead acid battery rating and model	24
3.5	DC-DC Boost Converter	27
3.6	Single phase Bridge inverter	28
<b>4. HYBRID SYSTEM CONTROL</b>		
4.1	Optimal Dispatch Controller	30
4.2	MPPT Controller	31
4.2.1.	MPPT for PV generator	31
4.2.2	MPPT for Wind generator	31
<b>5. SIMULATION MODELS AND RESULTS</b>		
5.1	MATLAB	34
5.1.1	Simulink	34
5.1.2	Power System Blockset	34
5.2	Simulation Model	35
5.2.1	Main circuit	35

5.2.2 MPPT Controller circuit	36
5.2.3 Single phase load	36
5.3 Simulation Results	38
5.3.1 Load Profile	38
5.3.2 Load Current	39
5.3.3 Comparison of load profile with Load current	39
5.3.4 Battery Status	40
<b>6. HARDWARE IMPLEMENTATION OF HYBRID SYTEM</b>	
6.1 Block diagram of Hybrid System	42
6.1.1 Rectifier part of Hybrid System	43
6.1.2 Inverter part of Hybrid System	44
6.1.3 Micro controller for Hybrid System	45
6.2 Photograph of hardware and result of Hybrid System	46
6.3 Hardware Results	47
6.3.1 Battery Condition	47
6.3.2 PWM Pulses	47
6.3.3 AC bus voltage	48
<b>7. CONCLUSION AND FUTURE SCOPE</b>	
7.1 Conclusion	50
7.2 Future Scope	50

<b>REFERENCES</b>	<b>51</b>
APPENDIX I	53
APPENDIX II	56
APPENDIX III	75

## LIST OF FIGURES

FIGURE	TITLE	PAGE NO
2.1	Smart grid Structure	7
3.1	Block Diagram of Hybrid Renewable Energy System	12
3.2.	Equivalent circuit of PV cell	14
3.3.	I-V and P-V characteristics for PV cell	15
3.4	Characteristics of I-V curve of PV cell.Net current I Composed of light generated current $I_{pv}$ and diode current $I_d$	16
3.5	$C_p$ vs $\lambda$ characteristics for wind turbine	22
3.6	Equivalent circuit and phasor diagram for PMSG	22
3.7	Equivalent circuit of Battery	25
3.8	Discharging characteristics of Battery	26
3.9	Charging characteristics of Battery	26
3.10	DC-DC Boost Converter Circuit	27
3.11	Waveform of Boost converter circuit	27
3.12	Single Phase inverter circuit	28
3.13	Single Phase inverter Gating Signal	28
4.1	Flow Chart of Optimal dispatch Controller	30
4.2	Circuit diagram for wind generator connected to DC bus	31
4.3	MPPT control loop	32



<b>FIGURE</b>	<b>TITLE</b>	<b>PAGE NO</b>
5.1	Simulation Circuit	35
5.2	MPPT Control block	36
5.3	Resistive Load	36
5.4	Load Profile	38
5.5	Load Current	39
5.6	Comparison of Load current with Load profile	40
5.7	Battery SOC Status	40
6.1	Hardware Block diagram	42
6.2	Schematic diagram of Hybrid system	43
6.3	Schematic of Power circuit	43
6.4	Schematic of single phase inverter	44
6.5	Schematic of driving circuit	45
6.6	Schematic of micro controller circuit	45
6.7	Photocopy of Hardware	46
6.8	Battery Charging Waveform	47
6.9	PWM Pulses for Boost Converter	47
6.10	PWM Pulse for Inverter	48
6.11	AC bus Voltage	48

## LIST OF TABLE

<b>TABLE</b>	<b>TITLE</b>	<b>PAGE NO.</b>
Table 1	Specification	37
Table 2	Load profile	38

## ABBREVIATIONS

DC	-	Direct Current
AC	-	Alternating Current
PWM	-	Pulse Width Modulation
PMSG	-	Permanent Magnet Synchronous Generator
SOC	-	State Of Charge
PV	-	Photo Voltaic
MPPT	-	Maximum Power Point Tracking
DOD	-	Depth Of Discharge

---

---

## CHAPTER 1

---

---

# CHAPTER 1

## 1. INTRODUCTION

### 1.1 INTRODUCTION OF HYBRID RENEWABLE SYSTEM

Smart Grid Energy Systems (SGES) is recently increasing, particularly onsite generation. This interest is because larger power plants are economically unfeasible in many regions due to increasing system and fuel costs, and more strict environmental regulations. In addition, recent technological advances in small generators, Power Electronics, and energy storage devices have provided a new opportunity for distributed energy resources at the distribution level.

Solar and wind energies, among other renewable energy sources, are the most available and distributed in all over the world. Applications with photovoltaic (PV) and wind have been increasing significantly due to the rapid growth of power electronic techniques. Generally, PV power and wind power are complementary since sunny days are usually calm and strong winds often occur on cloudy days or in night time. The hybrid PV-wind power system therefore has higher availability to deliver continuous power and results in a better utilization of power conversion and control equipment than either of the individual sources. Battery is used as a backup power. Every major component of the system is modeled, and then the control strategies are applied to the system. Fig. 2.1 shows a simple diagram of the different components of the hybrid system connected to the smart grid. The PV and Wind generator is controlled by a DC/DC boost converter, where the duty ratio is used as the control means to track the maximum power point. The power generated from the PV generator and wind is supplied to the DC bus bar, where a grid connected inverter is used to supply the total generated power to the load. The wind generator consists of a wind turbine directly driving a permanent magnet synchronous generator (PMSG) with a power electronic system that connects the wind turbine generator to the grid. The power electronic interface consists of an uncontrolled rectifier, a boost DC/DC converter and the grid inverter that is shared with the PV, wind generator and battery.

## **1.2 OBJECTIVES OF THE PROJECT**

The objective of the project is designing the Optimal dispatch controller, implements hybrid renewable system. The load power is balanced by renewable sources and battery. Here two renewable sources like solar and wind is implemented. To track the maximum power from solar and wind, MPPT controller is designed.

## **1.3 ORGANIZATION OF THESIS**

This gives an overall outline of the project report.

### **CHAPTER 1**

It describes the general introduction for Hybrid system and Smart grid.

### **CHAPTER 2**

It describes the Smart grid and benefits in Hybrid Renewable system.

### **CHAPTER 3**

It describes the Components and modeling of Hybrid Renewable energy system.

### **CHAPTER 4**

It describes the optimal dispatch controller and MPPT controllers.

### **CHAPTER 5**

It includes the introduction MATLAB (simulink), simulation details of individual block and simulation results of the system.

### **CHAPTER 6**

It includes the proposed system model and description of all components used in the hardware. It shows the schematic diagram of the hardware and output waveforms and test results.

### **CHAPTER 7**

It gives the conclusion and recommendations for the future work.

---

---

## CHAPTER 2

---

---

## CHAPTER 2

### SMART GRID

#### 2.1 INTRODUCTION OF SMART GRID

Most of the world's electricity delivery system or "grid" was built when energy was relatively inexpensive. While minor upgrades have been made to meet increasing demand, the grid still operates the way it did almost 100 years ago—energy flows over the grid from central power plants to consumers, and reliability is ensured by maintaining excess capacity.

The result is an inefficient and environmentally wasteful system that is a major emitter of greenhouse gases, consumer of fossil fuels, and not well suited to distributed, renewable solar and wind energy sources. In addition, the grid may not have sufficient capacity to meet future demand.

Several trends have combined to increase awareness of these problems, including greater recognition of climate change, commitments to reduce carbon emissions, rising fuel costs, and technology innovation. In addition, recent studies support a call for change:

- Power generation causes 25.9 percent of global carbon (CO<sub>2</sub>) emissions.
- CO<sub>2</sub> emissions from electricity use will grow faster than those from all other sectors through 2050
- Increase distributed solar and wind power generation to increase the electrical supply without additional greenhouse gas emissions
- Use plug-in hybrid electric vehicles (PHEVs) to generate and consume electric power intelligently
- Sequester (scrub and store) the carbon from coal plant emissions
- Use demand management to improve energy efficiency and reduce overall electricity consumption
- Monitor and control the energy grid in near-real time to improve reliability and utilization, reduce blackouts, and postpone costly new upgrades



- Rooftop solar panels need to notify backup power generators within seconds that approaching clouds will reduce output.
- The grid needs to notify PHEVs about the best time to recharge their batteries.
- Utility companies need to communicate with and control appliances such as refrigerators and air conditioners during periods of peak electricity demand.
- Factory operators must know the cost of electric power every few minutes to manage their energy use economically.
- Homeowners need to become smart buyers and consumers of electricity by knowing when to adjust thermostats to optimize energy costs.

Unfortunately, these activities cannot be achieved with the current energy grid. Today's electric infrastructure simply cannot coordinate and control all the systems that will be attached to it.

A new, more intelligent electric system, or "Smart Grid," is required that combines information technology (IT) with renewable energy to significantly improve how electricity is generated, delivered, and consumed. A Smart Grid provides utility companies with near-real-time information to manage the entire electrical grid as an integrated system, actively sensing and responding to changes in power demand, supply, costs, and emissions—from rooftop solar panels on homes, to remote, unmanned wind farms, to energy-intensive factories.

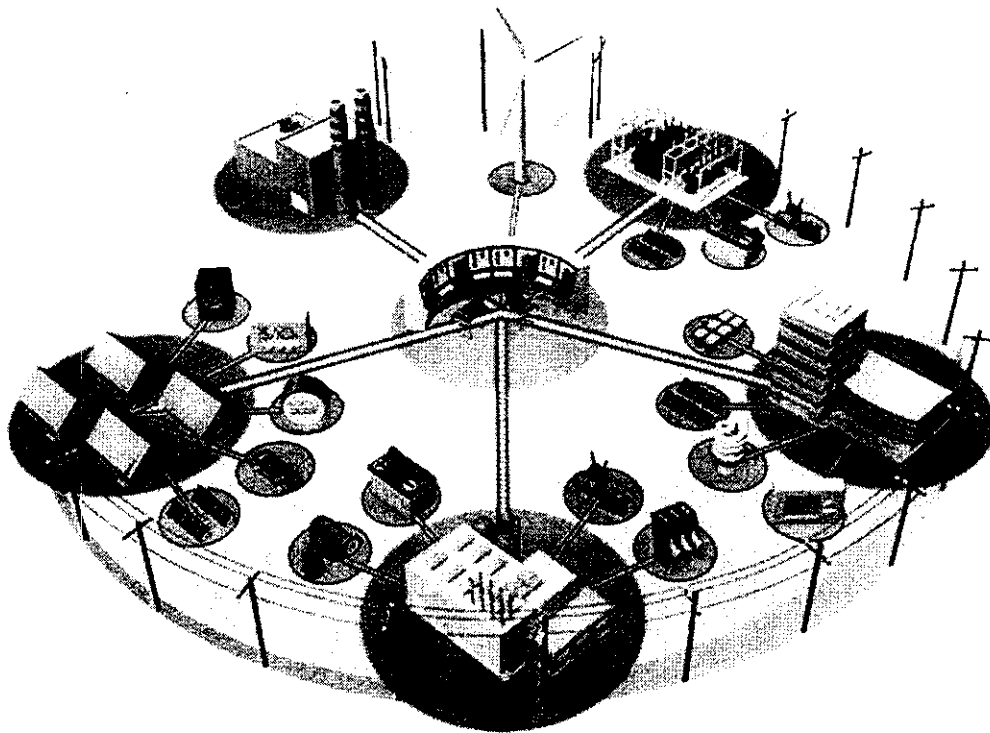


Fig 2.1 Smart grid structure

## 2.2 COMPONENTS OF A SMART GRID

A Smart Grid comprises three major components:

- 1) demand management,
- 2) distributed electricity generation, and
- 3) transmission and distribution grid management.

### 2.2.1 DEMAND MANAGEMENT:

Reducing Electricity Consumption in Homes, Offices, and Factories

Demand management works to reduce electricity consumption in homes, offices, and factories by continually monitoring electricity consumption and actively managing how appliances consume energy. It consists of demand-response programs, smart meters and

variable electricity pricing, smart buildings with smart appliances, and energy dashboards. Combined, these innovations allow utility companies and consumers to manage and respond to the variances in electricity demand more effectively.

- **Demand response**—During periods of peak energy use, utility companies send electronic alerts asking consumers to reduce their energy consumption by turning off non-essential appliances. When the Smart Grid is fully developed, alert signals will be automatically sent to appliances, eliminating the need for manual intervention.

If enough consumers comply with this approach, the reduction in power consumption could be enough to keep a typical utility company from building an additional power plant—the most expensive asset utility companies operate.<sup>4</sup> To increase the number of consumers who comply, utility companies may offer cash payments or reduce consumers' electric bills.

- **Smart meters and variable pricing**—Today's electricity prices on the wholesale market are volatile because they are determined by supply and demand, as well as by situations that depend on generation capacity, fuel prices, weather conditions, and demand fluctuations over time. On average, off-peak prices at night are 50 percent less than prices during the day. During demand peaks, prices can be many times greater than those of off-peak periods.

Despite price fluctuations in wholesale markets, most retail consumers are currently charged a flat price for electricity regardless of the time of day or actual demand. Consumers, therefore, have no visibility into when energy is in short supply, and have little incentive to lower their energy use to reduce their energy bill while helping utility companies meet demand. To remedy this situation, utility companies are now replacing traditional mechanical electric meters with smart meters. These new devices allow utility companies to monitor consumer usage frequently and, more important, give customers the ability to choose variable-rate pricing based on the time of day. By seeing the real cost of energy, consumers can respond accordingly by shifting their energy consumption from high-price to low-price periods. This process, called “load shifting” or “load shedding,” can have the joint benefit of reducing costs for typical consumers while lowering demand peaks for utility companies.

### **2.2.2 DISTRIBUTED ELECTRICITY GENERATION:**

Renewable energy using microgeneration devices—Already, some homes and offices find it cost-effective to produce some or all of their own electricity using microgeneration devices—small-scale energy-generation equipment designed for use in homes and offices. Microgeneration devices primarily include rooftop solar panels, wind turbines, fossil fuel cogeneration plants, and soon, PHEVs that can generate electricity for sale back to the grid.

These devices are becoming more affordable for residential, commercial, and industrial customers. Depending on the technology type and operating environment, microgeneration devices can be cost-competitive compared to conventional generation methods. Even so, widespread adoption of these technologies will require government incentives, public awareness campaigns, and further technology development.

When fully developed, a Smart Grid will allow owners of microgeneration devices and other energy-generation equipment to sell energy back to utility companies for a profit more easily. When this happens, consumers become an active part of the grid rather than being separate from it.

Despite the obvious benefits, renewable energy generation also provides a unique challenge: wind and solar power are much more variable than conventional power plants. For example, when the wind stops blowing or the sky becomes overcast, these systems stop generating power, creating shortages in the electrical grid. To compensate, utility companies must be able to anticipate these shortages in time to start up conventional power plants to temporarily offset the energy deficit. The Smart Grid will integrate weather reports, real-time output monitoring, and grid-load balancing to respond to this variability proactively.

### **2.2.3 TRANSMISSION AND DISTRIBUTION GRID MANAGEMENT**

Utility companies are turning to IT solutions to monitor and control the electrical grid in real time. These solutions can prolong the useful life of the existing grid, delaying major investments needed to upgrade and replace current infrastructure. Until now, monitoring has focused only on high-voltage transmission grids. Increasing overall grid reliability and utilization, however, will also require enhanced monitoring of medium- and low-voltage distribution grids.

- Grid monitoring and control—Expensive power outages can be avoided if proper action is taken immediately to isolate the cause of the outage. Utility companies are installing sensors to monitor and control the electrical grid in near-real time (seconds to milliseconds) to detect faults in time to respond. These monitoring and control systems are being extended from the point of transmission down to the distribution grid. Grid performance information is integrated into utility companies’ supervisory control and data acquisition (SCADA) systems to provide automatic, near-real-time electronic control of the grid.
- Grid security and surveillance—Many of the assets used to generate and transmit electricity are vulnerable to terrorist attacks and natural disasters. Substations, transformers, and power lines are being connected to data networks, allowing utility companies to monitor their security using live video, tamper sensors, and active monitoring.

### **BENEFITS OF SMART GRID**

1. Reliability — by reducing the cost of interruptions and power quality disturbances and reducing the probability and consequences of widespread blackouts
2. Economics — by keeping downward prices on electricity prices, reducing the amount paid by consumers as compared to the “business as usual” (BAU) grid, creating new jobs, and stimulating the our gross domestic product (GDP).
3. Efficiency — by reducing the cost to produce, deliver, and consume electricity
4. Environmental — by reducing emissions when compared to BAU by enabling a larger penetration of renewables and improving efficiency of generation, delivery, and consumption
5. Security — by reducing the probability and consequences of manmade attacks and natural disasters
6. Safety — by reducing injuries and loss of life from grid-related events

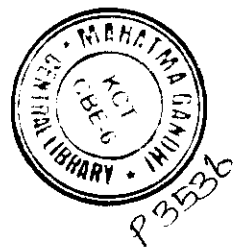
---

---

## CHAPTER 3

---

---



## CHAPTER 3

### COMPONENTS AND MODELING OF THE HYBRID SYSTEM

#### 3.1. BLOCK DIAGRAM OF HYBRID RENEWABLE SYSTEM:

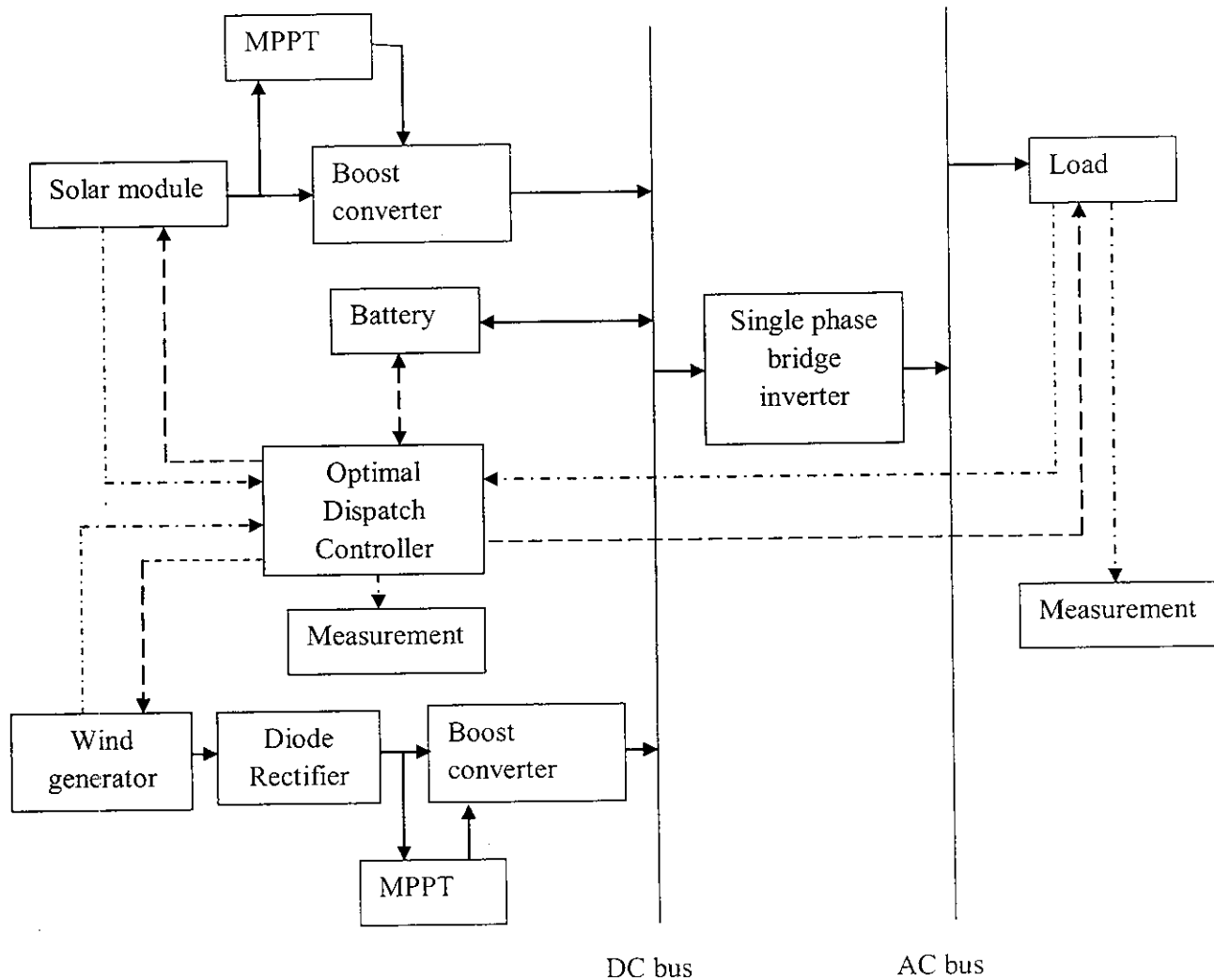


Fig 3.1 Block Diagram of Hybrid Renewable Energy System

From the block diagram describes overview of the project. The Solar array is modeled for different irradiation and temperature condition. To extracting the maximum power from solar, the power point tracking controller is employed. Different types of algorithm are present. Here Perturb and observe method were proposed. The gating signal are generated by PWM technique.

This gating signal given to boost DC to DC converter. This maintains constant dc voltage. Similar to that Wind turbine is modeled and Permanent Magnet Synchronous Generator(PMSG) is used to convert mechanical energy to electrical energy. A diode rectifier rectifies the ac to dc voltage. A maximum power point tracking is also used. A battery is used to supply the load when generation is less than load demand and surplus of power is stored in battery when generation is greater than load. An inverter is converts dc to ac voltage. A load is connected to AC bus. An optimum controller is used control of power. That is generation is greater than load the surplus power stored in battery. If generation is less than load demand , the shortage of power is taken from battery. Here five different types of load connected to AC bus. Depends upon source power particular load is connected to bus and it is controlled by optimal dispatch controller. Suppose source power is low, due to load balance , particular load tripped. A measurement system shows the generation, load power ,Battery condition for Smart grid application.

#### **BENEFITS OF HYBRID RENEWABLE SYSTEM:**

The main benefits (advantages) of a hybrid system can be summarized as :

1. The possibility to combine two or more renewable energy sources, based on the natural local potential of the users.
2. Environmental protection especially in terms of CO<sub>2</sub> emissions reduction.
3. Low cost – wind energy, and also solar energy can be competitive with nuclear, coal and gas especially considering possible future cost trends for fossil and nuclear energy.
4. Diversity and security of supply.
5. Rapid deployment - modular and quick to install.
6. Fuel is abundant, free and inexhaustible.
7. Costs are predictable and not influenced by fuel price fluctuations although fluctuations in the price of batteries will be an influence where these are incorporated.



### 3.2 MODELING OF SOLAR CELL:

#### 3.2. 1. IDEAL PHOTOVOLTAIC CELL

The equivalent circuit of the ideal photovoltaic cell is,

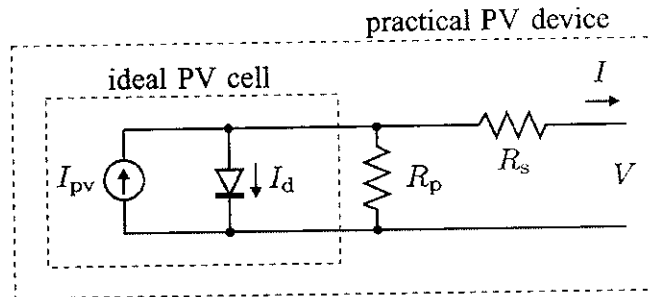


Fig 3.2 Equivalent circuit of pv cell

The basic equation from the theory of semiconductors that mathematically describes the I-V characteristic of the ideal photovoltaic cell is:

$$I = I_{pv, cell} - I_{o, cell} \left[ \exp\left(\frac{qV}{akT}\right) - 1 \right] \quad (1)$$

Where

$I_{pv, cell}$  = current generated by the incident light (it is directly proportional to the Sun irradiation),

$I_{o, cell}$  = reverse saturation or leakage current of the diode

$q$  = electron charge ( $1.6 \times 10^{-19} \text{C}$ )

$k$  = Boltzmann constant ( $1.3806503 \times 10^{-23} \text{ J/K}$ ),

$T$  = Temperature of the  $p-n$  junction

$a$  = diode ideality constant, data at [1],[2]

#### 3.2. 2. MODELING THE PHOTOVOLTAIC ARRAY

The basic equation (1) of the elementary photovoltaic cell does not represent the I-V characteristic of a practical photovoltaic array. Practical arrays are composed of several connected photovoltaic cells and the observation of the characteristics at the terminals of the photovoltaic array requires the inclusion of additional parameters to the basic equation

$$I = I_{pv} - I_0 \left[ \exp \left( \frac{V + R_s I}{V_{ta}} \right) - 1 \right] - \frac{V + R_s I}{R_p} \quad (2)$$

where

$I_{pv}$  = the photovoltaic

$I_0$  = saturation currents of the array

$V_t = N_s k T / q$  = Thermal voltage of the array

$N_s$  cells connected in series.

Cells connected in parallel increase the current and cells connected in series provide greater output voltages. If the array is composed of  $N_p$  parallel connections of cells the photovoltaic and saturation currents may be expressed as:  $I_{pv} = I_{pv, cell} N_p$ ,  $I_0 = I_{0, cell} N_p$ .  $R_s$  is the equivalent series resistance of the array and  $R_p$  is the equivalent parallel resistance.

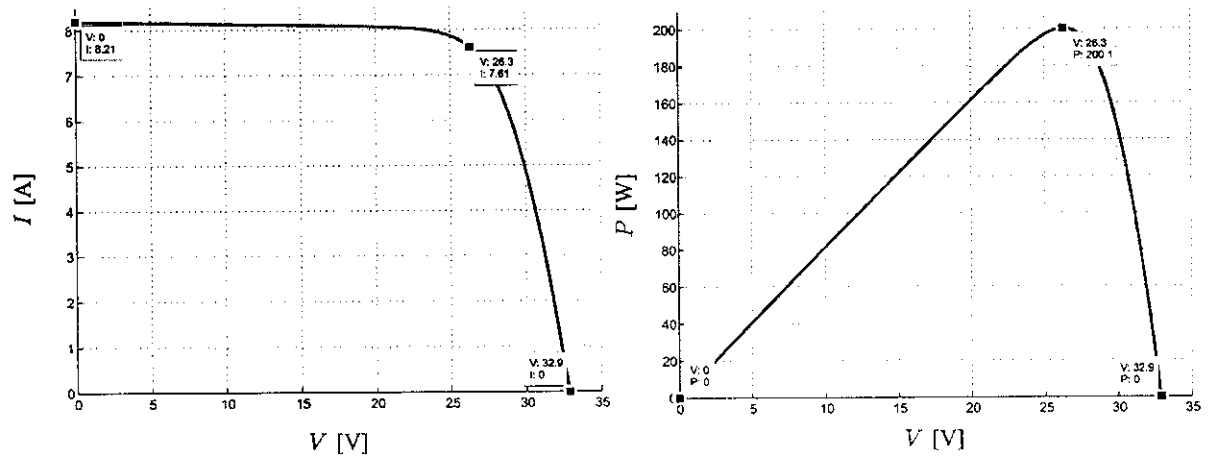


Fig 3.3 I-V and P-V characteristics for PV cell

The equation originates the I-V curve, where three *remarkable points* are highlighted: short circuit (0,  $I_{sc}$ ), maximum power point ( $V_{mp}$ ,  $I_{mp}$ ) and open-circuit ( $V_{oc}$ , 0).. In a three-diode model is proposed to include the influence of effects which are not considered by the previous models. For simplicity the single-diode model. This model offers a good compromise between simplicity and accuracy and has been used by several authors in previous works, sometimes with simplifications but always with the basic structure composed of a current source and a parallel diode . The simplicity of the single-diode model is used.

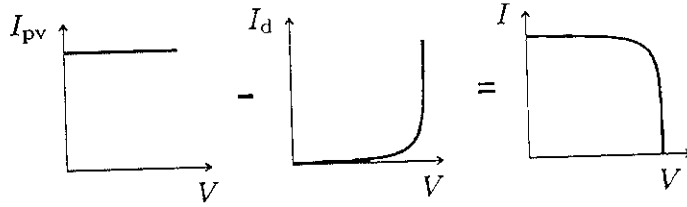


Fig 3.4 Characteristics of I-V curve of PV cell. Net current  $I$  composed of light generated current  $I_{pv}$  and diode current  $I_d$

Manufacturers of photovoltaic arrays, instead of the I-V equation, provide only a few experimental data about electrical and thermal characteristics. Unfortunately some of the parameters required for adjusting photovoltaic array models cannot be found in the manufacturer's data sheets, such as the light-generated or photovoltaic current, the series and shunt resistances, the diode ideality constant, the diode reverse saturation current, and the band gap energy of the semiconductor. All photovoltaic array datasheets bring basically the following information: the nominal open-circuit voltage  $V_{oc,n}$ , the nominal short-circuit current  $I_{sc,n}$ , the voltage at the maximum power point  $V_{mp}$ , the current at the maximum power point  $I_{mp}$ , the open-circuit voltage/temperature coefficient  $K_V$ , the short-circuit current/temperature coefficient  $K_I$ , and the maximum experimental peak output power  $P_{max,e}$ . This information is always provided with reference to the nominal or standard test conditions (STC) of temperature and solar irradiation. Some manufacturers provide I-V curves for several irradiation and temperature conditions. These curves make easier the adjustment and the validation of the desired mathematical I-V equation. Basically this is all the information one can get from datasheets of photovoltaic arrays.

Electric generators are generally classified as current or voltage sources. The practical photovoltaic device presents an hybrid behavior, which may be of current or voltage source depending on the operating point, as shown in Fig. 3.3. The practical photovoltaic device has a series resistance  $R_s$  whose influence is stronger when the device operates in the voltage source region and a parallel resistance  $R_p$  with stronger influence in the current source region of operation. The  $R_s$  resistance is the sum of several structural resistances of the device [3]. The  $R_p$  resistance exists mainly due to the leakage current of the  $p-n$  junction and depends on the

fabrication method of the photovoltaic cell. The value of  $R_p$  is generally high The value of  $R_s$  is very low and sometimes this parameter is neglected.

The I-V characteristic of the photovoltaic device shown in Fig. 3.2 depends on the internal characteristics of the device ( $R_s$ ,  $R_p$ ) and on external influences such as irradiation level and temperature. The amount of incident light directly affects the generation of charge carriers and consequently the current generated by the device. The light-generated current ( $I_{pv}$ ) of the elementary cells, without the influence of the series and parallel resistances, is difficult to determine. Datasheets only inform the nominal short-circuit current ( $I_{sc,n}$ ), which is the maximum current available at the terminals of the practical device. The assumption  $I_{sc} = I_{pv}$  is generally used in photovoltaic models because in practical devices the series resistance is low and the parallel resistance is high. The light generated current of the photovoltaic cell depends linearly on the solar irradiation and is also influenced by the temperature according to the following equation ,(being  $T$  and  $T_n$  the actual and nominal temperatures [K]),  $G$  [W/m<sup>2</sup>] is the irradiation on the device surface, and  $G_n$  is the nominal irradiation.

$$I_{pv} = (I_{pv,n} + Kt\Delta T) \frac{G}{G_n} \quad (3)$$

The diode saturation current  $I_0$  and its dependence on the temperature may be expressed by

$$I_0 = I_{0,n} \left(\frac{T_0}{T}\right)^3 \exp\left[\frac{qE_g}{ak} \left(\frac{1}{T_0} - \frac{1}{T}\right)\right] \quad (4)$$

where  $E_g$  is the bandgap energy of the semiconductor ( $E_g \approx 1.12$  eV for the polycrystalline Si at 25 °C [4], [6]), and  $I_{0,n}$  is the nominal saturation current:

$$I_{0,n} = \frac{I_{sc,n}}{\exp\left(\frac{V_{oc,n}}{aV_{t,n}}\right) - 1} \quad (5)$$

with  $V_{t,n}$  being the thermal voltage of  $N_s$  series-connected cells at the nominal temperature  $T_n$ . The saturation current  $I_0$  of the photovoltaic cells that compose the device depend on the saturation current density of the semiconductor ( $J_0$ , generally given in [A/cm<sup>2</sup>]) and on the effective area of the cells. The current density  $J_0$  depends on the intrinsic characteristics of the photovoltaic cell, which depend on several physical parameters such as the coefficient of diffusion of electrons in the semiconductor, the lifetime of minority carriers, the intrinsic carrier

density. This kind of information is not usually available for commercial photovoltaic arrays. In this paper the nominal saturation current  $I_{0,n}$  is indirectly obtained from the experimental data through  $I_0$  equation, which is obtained by evaluating  $I$  equation at the nominal open-circuit condition, with  $V = V_{oc,n}$ ,  $I = 0$ , and  $I_{pv} = I_{sc,n}$ .

The value of the diode constant  $a$  may be arbitrarily chosen. Many authors discuss ways to estimate the correct value of this constant [7], [8]. Usually  $a$  (1 to 1.5) and the choice depends on other parameters of the I-V model. Some values for  $a$  are found in based on empirical analysis. As reference says, there are different opinions about the best way to choose  $a$ . Because  $a$  expresses the degree of ideality of the diode and it is totally empirical, any initial value of  $a$  can be chosen in order to adjust the model. The value of  $a$  can be later modified in order to improve the model fitting if necessary. This constant affects the curvature of the I-V characteristic and varying  $a$  can slightly improve the model accuracy.

### 3.3 MODELING OF WIND ENERGY

#### 3.3.1. MECHANICAL POWER EXTRACTION FROM THE WIND

The blades of a wind turbine extract the energy flow from moving air, which then converts this energy to rotational energy and delivers it via a mechanical drive unit to the rotor of an electric generator. The kinetic energy in air of an object of mass  $m$  moving with speed  $v$  is equal to:

$$E = \frac{1}{2}mV^2 \quad (6)$$

The power in the moving air, if we assume constant wind velocity, is

$$P_{wind} = \frac{dE}{dT} = \frac{1}{2}mV^2 \quad (7)$$

where  $m$  is the mass flow rate per second. When the air passes across an area  $A$ , such as the area swept by the rotor blades, the power in the air can be estimated:

$$P_{wind} = \frac{1}{2}\rho AV^3 \quad (8)$$

where  $\rho$  is the air density. The air density varies with air pressure and temperature, therefore  $\rho = 1.225 \text{ kg/m}^3$  for the purpose of this thesis.

The equation above estimates how much power there is in the wind, but how much of this power can be extracted from the airstream with an energy converter? the mechanical energy which the converter extracts from the airflow will be equal to the power difference of the air stream before and after the converter:

$$P_{\text{mech}} = \frac{1}{2} \rho A_1 V_1^3 - \frac{1}{2} \rho A_2 V_2^3 = \frac{1}{2} \rho A_1 V_1^3 - A_2 V_2^3 \quad (9)$$

where  $A_1$  and  $A_2$  are the cross-sectional areas before and after the converter, and  $v_1$  and  $v_2$  are the wind speed before and after the converter. As the airflow passes through the converter the wind velocity behind the wind energy converter must decrease and the mass flow remains unchanged. Therefore,

$$\rho V_1 A_1 = \rho V_2 A_2 \quad (10)$$

$$P_{\text{mech}} = \frac{1}{2} \rho A_1 V_1 V_1^2 - V_2^2 \quad (11)$$

From the above equation we can see that the maximum mechanical power occurs when  $v_2$  is zero. If  $v_2$  equals zero, the air was brought to a complete stop by the converter, which is not physically possible. If the outflow velocity behind the converter is zero, then the inflow velocity must be zero, which implies that there is no flow through the converter. Therefore, the mechanical power extracted from the air stream must be expressed from another equation. Using the law of conservation of momentum, the force exerted by the wind onto the converter is:

$$F = mV_1 - V_2 \quad (12)$$

and the extracted mechanical power is:

$$P_{\text{mech}} = Fv^1 = mv_1 - v_2 v^1 \quad (13)$$

By comparing equation 2.4 and 2.8 we will be able to obtain the relationship for the flow velocity  $v^1$ :

$$v^1 = \frac{1}{2} v_1 - v_2 \quad (14)$$

Thus the velocity of the airflow through the converter is equal to the average of  $v_1$  and  $v_2$ . The mechanical power output of the converter can then be expressed as:

$$P_{\text{mech}} = \frac{1}{4} \rho A V_1^2 - V_2^2 V_1 \div V_2 \quad (15)$$

if comparing this mechanical power output with the power in the air stream that flows through the same cross-sectional area  $A$ , the ratio between the mechanical power extracted by the

converter and the power contained in the air stream that passes through the same area is called the “power coefficient”  $c_p$  and can be represented as follows

$$C_p = \frac{P_{mech}}{P_{wind}} = \frac{1/4\rho A(v_1^2 - v_2^2)(v_1 + v_2)}{1/2\rho A v_1^3} \quad (16)$$

the power coefficient can also be express in terms of the velocity ratio  $v_1/v_2$ :

$$C_p = \frac{P_{mech}}{P_{wind}} = 1/2 \left[ 1 - \left( \frac{v_2}{v_1} \right)^2 \right] \left[ 1 + \frac{v_2}{v_1} \right] \quad (17)$$

If we plot equation (2.12) we will see that the maximum ideal power coefficient  $C_p$  happens when  $v_1/v_2=1/3$  (see Fig. 3.4), therefore  $C_p$  becomes

$$C_p = 16/27 = 0.593$$

This was first derived by A. Betz, and it is called the “Betz factor” or “Betz limit” [9]. This value is the maximum theoretical value of the power coefficient, therefore, the maximum theoretical efficiency that a wind energy converter can have is 59.3%. It is good to mention that this value of the power coefficient was obtained for an ideal, frictionless flow converter. In real cases, the wind turbine will always have a smaller maximum power coefficient than the Betz factor; this is due to many aerodynamic losses that depend on the rotor design and construction (number of blades, weight, stiffness, etc). The power coefficient and the efficiency of a wind turbine system are different. The efficiency of a wind turbine includes the loss in the mechanical transmission, electrical generation, converter loss, etc., where as the power coefficient is the efficiency of converting the power in the wind into mechanical energy in the rotor shaft. The power coefficient is usually given as a function of the tip speed ratio  $\lambda$  and the blade pitch angle  $\beta$ . The pitch angle is the angle between the plane of rotation and the blade cross-section chord. The tip speed ratio of a wind turbine is defined as

$$\lambda = \frac{u}{v_1} = \frac{\omega R}{v_1} \quad (18)$$

Where  $u$  is the tangential velocity of the blade pitch,  $\omega$  is the angular velocity of the rotor,  $R$  is the rotor radius in meters, and  $v_1$  is the wind speed. The graph of the power coefficient versus the tip speed ratio is given in Fig.3. 4. This graph is a key element in the characterization of wind energy converters [10].

### 3.3. 2. ROTOR POWER CHARACTERISTICS

The wind power mainly depends on geographic and weather conditions and varies from time-to-time. Therefore it is necessary to construct a system that can generate maximum power for all operating conditions. Recently, permanent magnet synchronous generator (PMSG) is used for wind power Generating system because of its advantages such as better reliability, lower maintenance, and more efficient

The generator is actually dedicated to a vertical axis wind turbine. Using a diode rectifier simplifies the structure and reduces system cost (no position sensor and low-cost converter without control).

The expression of the output power is where:

$$P_m = \frac{1}{2} \rho A V^3 C_p \quad (19)$$

- $P_m$ : Mechanical output power of the turbine (W),
- $C_p$ : Performance coefficient of the turbine,
- $\rho$ : Air density (Kg/m<sup>3</sup>),
- $A$ : Turbine swept area (m<sup>2</sup>),
- $V$ : Wind speed (m/s).

For a giving wind turbine, as the two parameters  $\rho$  and  $A$  are constants, the value of the output power depends on the performance coefficient  $C_p$  and the wind speed. To maximize this output power, and as the wind speed is varying from time to time, the performance coefficient must be maximized [11],[12]. Therefore, it must be controlled. Its expression is

$$C_p(\lambda, \beta) = C_1 \left( \frac{C_2}{\lambda_i} - C_3 \beta - C_4 \right) \exp \left( -\frac{C_5}{\lambda_i} \right) + C_6 \lambda_i \quad (20)$$

$\lambda$  =tip speed ratio of rotor blade tip speed to wind speed

$\beta$ =the blade pitch angle

$$\frac{1}{\lambda_i} = \frac{1}{\lambda + 0.08\beta} - \frac{0.035}{\beta^2 + 1} \quad (21)$$

$$C_1=0.5176 \quad C_2=116 \quad C_3=0.4 \quad C_4=5 \quad C_5=21 \quad C_6=0.0068$$



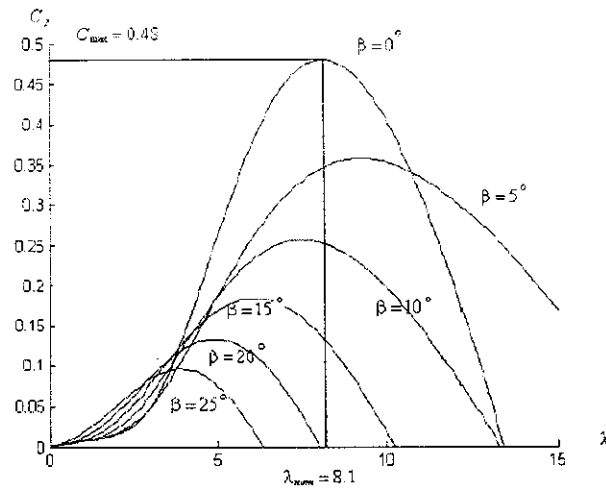


Fig 3.5 Cp vs lambda characteristics for wind turbine

**3.3.3 .PERMANENT MAGNET SYNCHRONOUS GENERATOR MODEL:**

Since the power for excitation source is not required for the permanent magnet synchronous generator, high efficiency is expected. And, since the electromotive force in proportion to rotational speed is generated, it is possible to take out the generated output in the easiness. The equivalent circuit and a phasor diagram for one phase are Represented

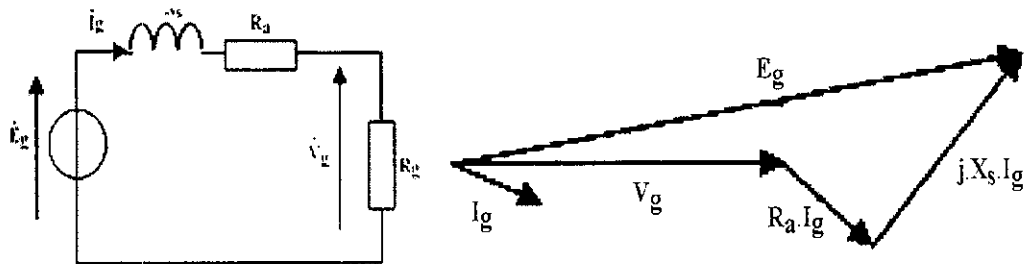


Fig 3.6 Equivalent circuit and phasor diagram for PMSG

When line current of the generator is defined as  $I_g$  the terminal voltage  $V_g$  of the generator is

$$V_g = E_g - jX_s * I_g - R_a * I_g \tag{22}$$

where  $R_a$  is the winding resistance per phase and  $X_s$  is the synchronous reactance per

$$I_g = \frac{E_g}{(R_g + R_a) + jX_s} \quad (23)$$

The amplitude of the line current is expressed as

$$|I_g| = \frac{|E_g|}{\sqrt{(R_a + R_g)^2 + X_s^2}} \quad (24)$$

The generated output power is

$$P = 3|I_g||V_g| \cos\phi = 3R_g * |I_g|^2 \quad (24)$$

$$P = 3R_g * \frac{E_g^2}{(R_g + R_a)^2 + X_s^2} \quad (25)$$

### 3.4. MODELING OF LEAD-ACID BATTERY:

A lead acid battery in its basic construction is made of more than one electrochemical cells interconnected in such a way to provide the required voltage and current. Lead acid battery is constructed of two electrodes, the positive one consists of lead dioxide  $PbO_2$  and the negative consists of pure lead (Pb). The empty space between the two electrodes is filled with diluted sulphuric acid ( $H_2SO_4$ ). The voltage of the battery depends on cell temperature and the density of the acid solution, also its density changes with temperature and charge state.

The depth of discharge (DOD) is the state of charge of the battery. The relation between battery voltage and its depth of discharge is almost linear until a cut-off-voltage point is reached. Operating battery beyond this point will result in increasing the internal resistance of the battery and may result in damaging of it. A charge controller (regulator) is used to control operation of battery within its design limits so that not to exceed its cut-off point, also not to exceed overcharge limit. A lead acid battery loses some of its capacity due to internal chemical reaction. This phenomenon is called self of discharge (SOD) of the battery and it increases with increasing in battery temperature. Providing batteries with lead grid or lead-calcium grid will minimize its SOD [13]. Long life-time, cycling stability rate and capability of standing very deep discharge are the main design points shall be taken into account when choose a battery for certain application.

### 3.4. 1. LEAD ACID BATTERY RATING AND MODEL

Battery rating is commonly specified in terms of its Ampere-hour (Ah) or Watt-hour (Wh) capacity. The ampere-hour capacity of a battery is the quantity of discharge current available for a specified length of time at a certain temperature and discharge rate. High discharge current would result in reduction of the battery capacity and will decrease its life time. The ampere-hour efficiency of a battery (nAh) is the ratio of amount of total Ampere-hours the battery provides during discharge to that required to charge it back to its original condition. The battery efficiency can be specified as Watt-hour efficiency (nWh) , its definition is in the same manner as nAh. nWh has values lower than nAh because the variation in voltage is taken into account [13] .

When the power generated from the renewable system (wind and PV in the case under study) exceeds the load requirement, energy is stored in the battery. A minimum storage level is specified for a battery so that should not be exceeded it. This level is a function of battery DOD so that

$$E_{min} = EBN * (1 - DOD) \quad (26)$$

where

$E_{min}$ : minimum allowable capacity of the battery bank,

EBN: is the nominal capacity of battery bank,

DOD : is the depth of discharge.

Energy stored in the battery at any time during charging mode can be expressed ,

$$E_b(t) = E_b(t-1) * (E_w(t) + E_{pv}(t) - E_l(t)/nV) * nWh \quad (27)$$

Energy stored in the battery at any time during discharging mode can be expressed ,

$$E_b(t) = E_b(t-1) * \left( 1 - \sigma - \left( \frac{E_l(t)}{nV} - (E_w(t) - E_{pv}(t)) \right) \right) \quad (28)$$

where  $E_b(t)$  and  $E_b(t-1)$ : are the charge capacity of battery bank at the time  $t$  and  $(t-1)$  respectively,

$\sigma$  : is hourly self discharge rate,

$EW(t)$  : is the energy from wind turbine during the time interval,

$EPV(t)$  : is the energy from PV system during the time interval,

$EL(t)$  : is the load requirement during the time interval,

$n_v$  and  $n_{wh}$  : are the efficiency of inverter and battery bank respectively as stated before.

The Battery block implements a generic model parameterized to represent most popular types of rechargeable batteries.

The equivalent circuit of the battery is shown below:

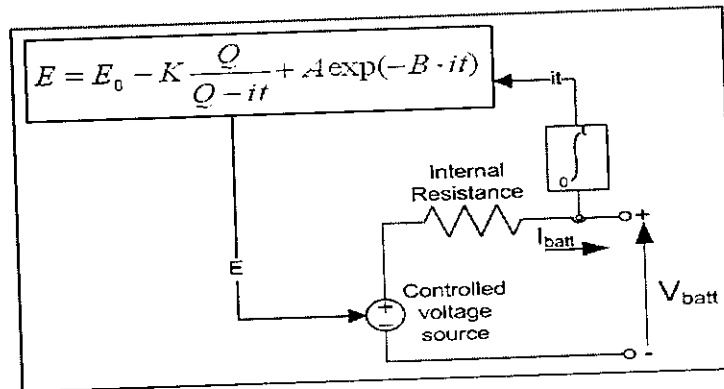


Fig 3.7 Equivalent circuit of Battery

where,  $E$  = No load voltage (V)

$E_0$  = Constant voltage (V)

$K$  = Polarization voltage (V)

$Q$  = Battery capacity (Ah)

$A$  = Exponential voltage (V)

$B$  = Exponential capacity (Ah)<sup>-1</sup>

All the parameters of the equivalent circuit can be modified to represent a particular battery type, based on its discharge characteristics. A typical discharge curve is composed of three sections:

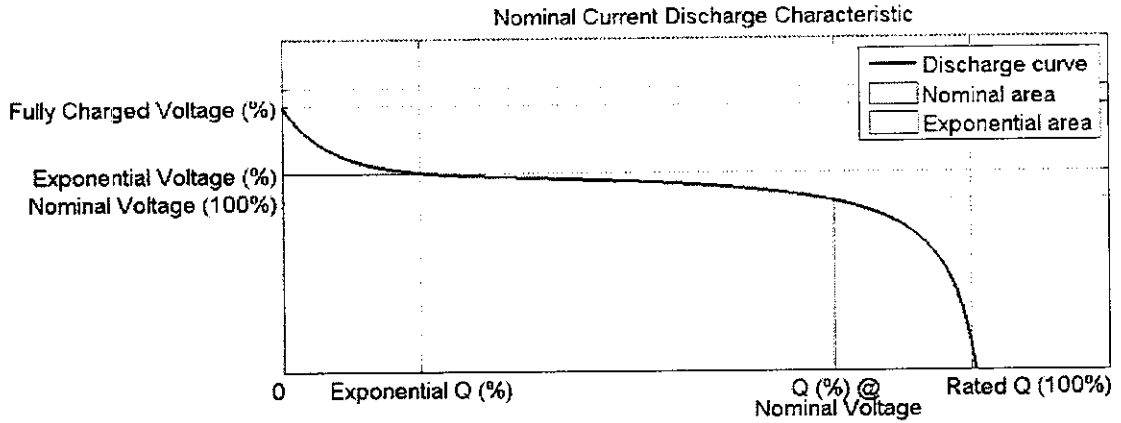


Fig 3.8 Discharging characteristics of Battery

The first section represents the exponential voltage drop when the battery is fully charged. The width of this region depends on the battery type. The second section represents the charge that can be extracted from the battery until the voltage drops below the battery nominal voltage. Finally, the third section represents the total discharge of the battery, when the voltage drops rapidly. When the battery current is negative, the battery will recharge following a charge characteristics

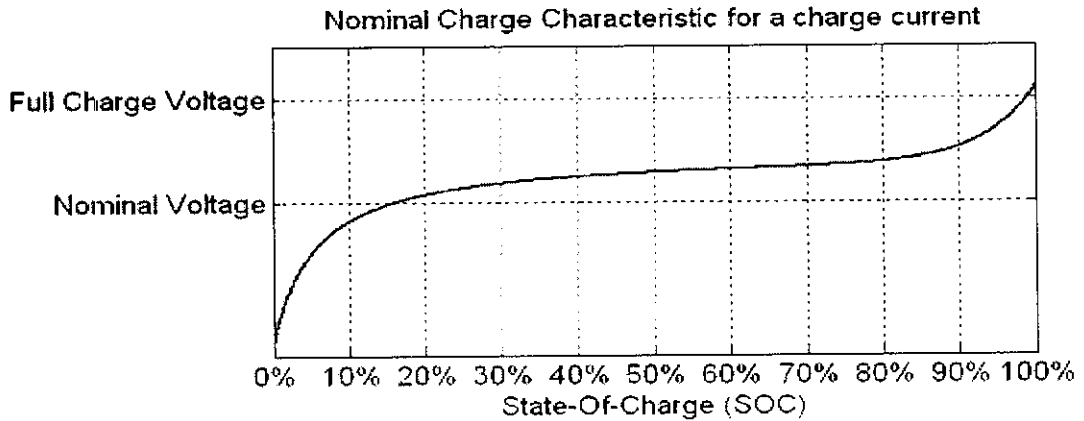


Fig 3.9 Charging characteristics of Battery

### 3.5. DC-DC BOOST CONVERTER

The Boost converter can be implemented in MPPT system where the output voltage of the system is required to be higher than the input.

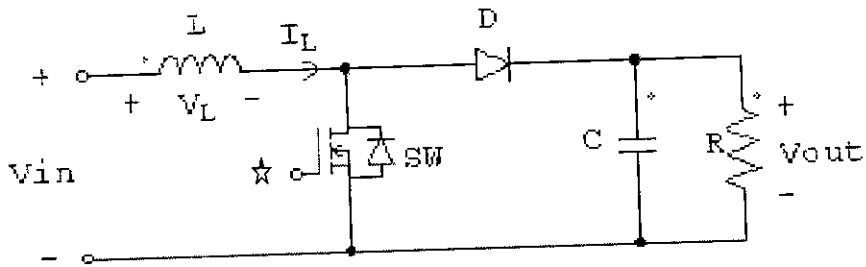


Fig 3.10 DC-DC Boost Converter Circuit

☆ Gate pulse from MPPT Controller

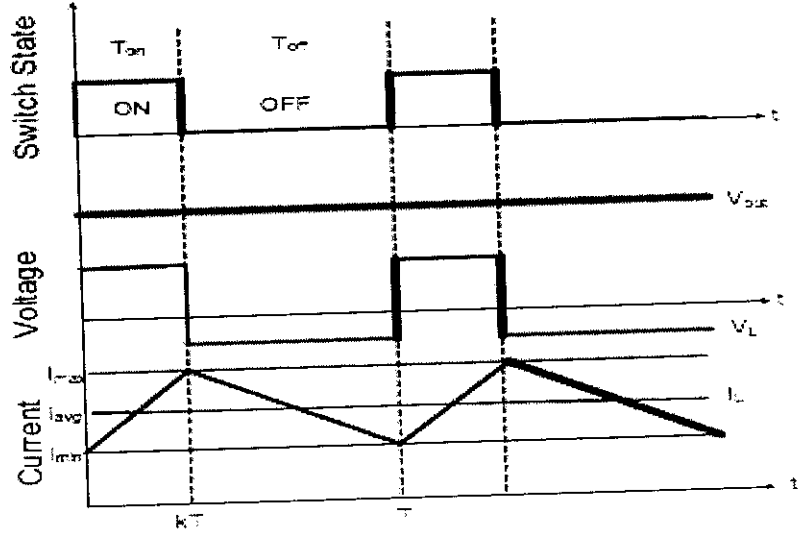


Fig 3.11 Waveform of Boost converter circuit

### 3.6. SINGLE PHASE BRIDGE INVERTER

A single phase full bridge inverter is used, the gate pulses are generated from pwm generator. In pwm generator, sinusoidal pulse width modulation is used

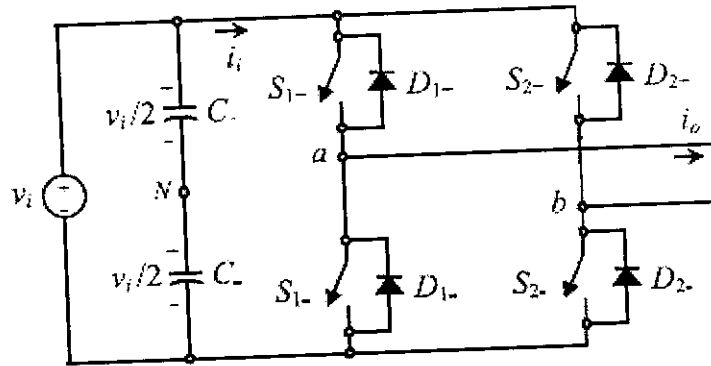


Fig. 3.12. Single Phase inverter circuit

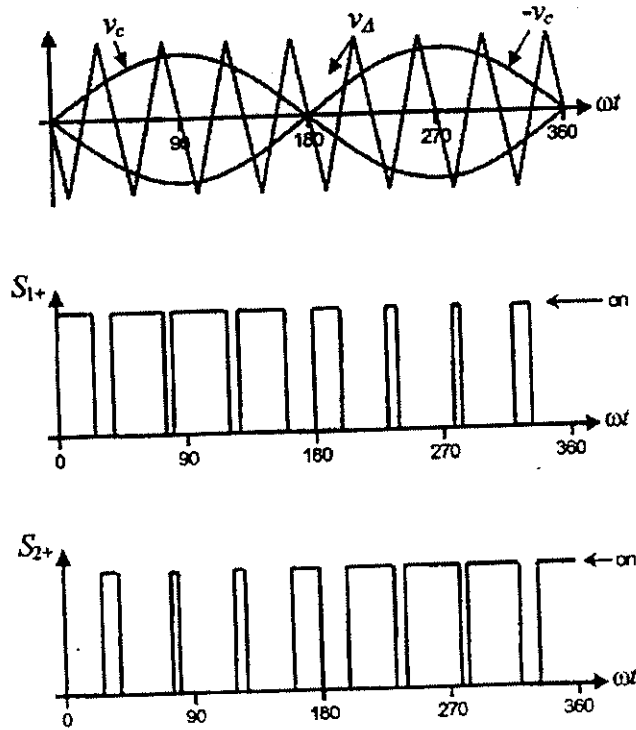


Fig. 3.13. Single Phase inverter Gating Signal

---

---

## CHAPTER 4

---

---



## CHAPTER 4

### HYBRID SYSTEM CONTROL

#### 4.1. OPTIMUM DISPATCH CONTROLLER:

The optimum dispatch controller controls the flow of power. The input of controller is solar current, wind generator current, Load current, battery current and battery SOC (state of charge). The total current (solar and wind) is greater than load current, the battery takes the current and remaining stores the battery. If SOC of battery greater than 0.8 the battery disconnected otherwise it stores the current. If total current is less than generated current shortage of current supplies by battery when SOC is greater than 0.3. If battery SOC reaches 0.3 the battery should be disconnected and also some amount of load is tripped.

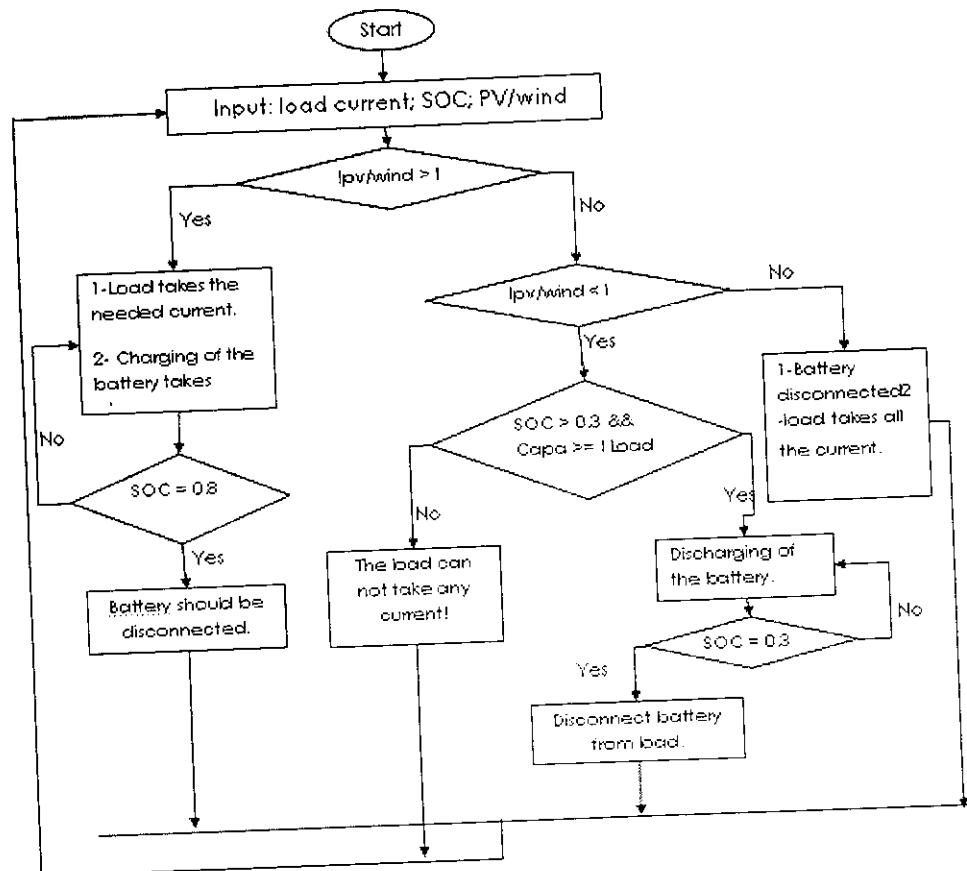


Fig 4.1 Flow Chart of Optimal dispatch Controller

## 4.2 MPPT CONTROLLER

Maximum power point tracking (MPPT) controllers are proposed to make the wind and the PV generators work in the maximum power mode that increases the energy captured from the wind speed and the solar radiation.

### 4.2.1. MPPT FOR PV GENERATOR

The PV generator is a DC source, with its output characteristics depending on the solar radiation temperature and the load condition. To maximize the output power of the PV generator, a maximum power point tracking controller is implemented in the system. The controller proposed by measuring only the current in the output of the DC/DC converter. Due to the constant DC bus bar voltage in the output of the boost converter" the Power can be maximized by maximizing the boost Converter output current. This method is simple and suitable for this application [14]

### 4.2.2. MPPT FOR WIND GENERATOR

The wind generator is an AC source of power, with its characteristics nonlinearly changing with wind speed and load condition. An MPPT controller is also implemented to maximize the output power of the wind generator. The DC/DC boost converter is used to maximize the power by measuring the DC output voltage of the rectifier ( $V_{boosew}$ ) at the input of the boost converter and according to the curve fitting of the power. against voltage ( $P_{mpp}-V_{mmp}$ ) characteristics; the maximum power is obtained. A block diagram showing the maximum power point tracking control loop is shown in Fig. 5 [15].

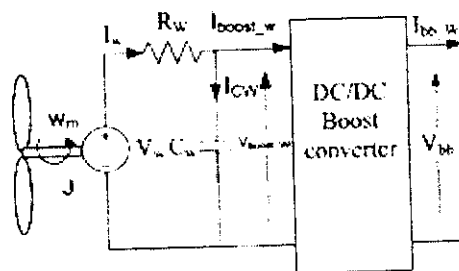


Fig.4.2. Circuit diagram for wind generator connected to DC bus

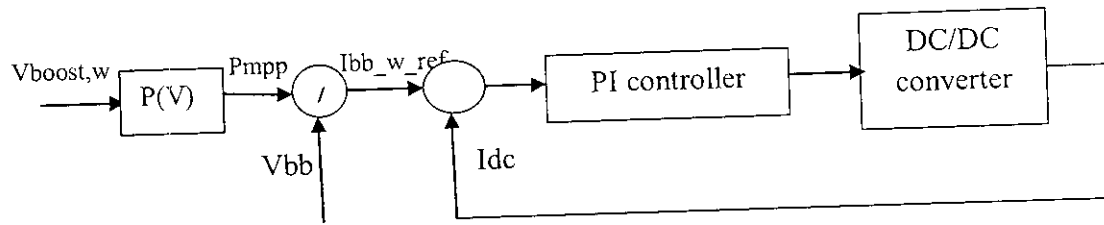


Fig. 4.3.MPPT control loop

---

---

## CHAPTER 5

---

---

## CHAPTER 5

### SIMULATION MODELS AND RESULTS

#### 5.1 MATLAB

The name MATLAB stands for matrix laboratory. MATLAB is a high-performance language for technical computing. It Integrates computation, visualization, and programming in an easy-to-use environment where problems and solutions are expressed in familiar mathematical notation. In this project the modelling and simulation of the proposed system is done using MATLAB (using simulink and power system block set tool boxes).

##### 5.1.1.SIMULINK

Simulink is a software package for modeling, simulating, and analyzing non linear dynamical systems. It is a graphical mouse-driven program that allows somebody to model a system by drawing a block diagram on the screen and manipulating it dynamically. Simulink is a platform for multi domain simulation and Model-Based Design for dynamic systems. It provides an interactive graphical environment and a customizable set of block libraries, and can be extended for specialized applications.

##### 5.1.2.POWER SYSTEM BLOCK SET

The Power System Block set allows scientists and engineers to build models that simulate power systems. The block set uses the Simulink environment, allowing a model to be built using click and drag procedures. Not only can the circuit topology be drawn rapidly, but also the analysis of the circuit can include its interactions with mechanical, thermal, control, and other disciplines. SimPowerSystems extends Simulink with tools for modelling and simulating basic electrical circuits and detailed electrical power systems. These tools let you model the generation, transmission, distribution, and consumption of electrical power, as well as its conversion into mechanical power. Sim Power Systems is well suited to the development of complex, self-contained power systems, such as those in automobiles, aircraft, manufacturing plants, and power utility applications

## 5.2 SIMULATION MODEL

### 5.2.1 MAIN CIRCUIT

The proposed system simulation circuit is shown in fig 5.1. From this circuit solar and wind is two major sources and battery is storage device. The total system was simulated for 6kW. The MPPT was implemented for both solar and wind, this is due to track the maximum power. MPPT controller takes the current as reference. The gate signal generated by MPPT controller and this gate pulses given to boost converter. Solar and wind connected to dc bus and also battery too connected. A single phase bridge inverter converts dc to ac. Here we use five different type of load. A controller decides which sources available and optimal use of sources

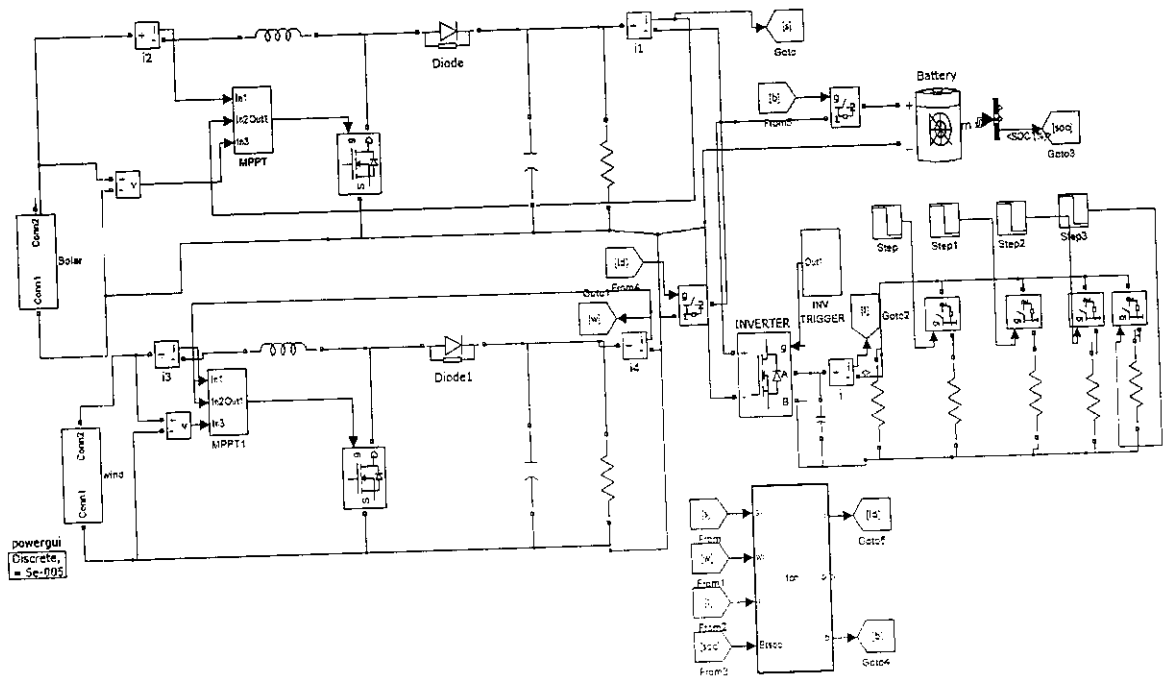


Fig 5.1 Simulation Circuit

### 5.2.2 MPPT CONTROLLER CIRCUIT

The control block is shown in fig 5.2. Here pi controller is used, it process the error signal. The error is generated by comparing reference current with output current. A gate pulse is generated and given to boost converter.

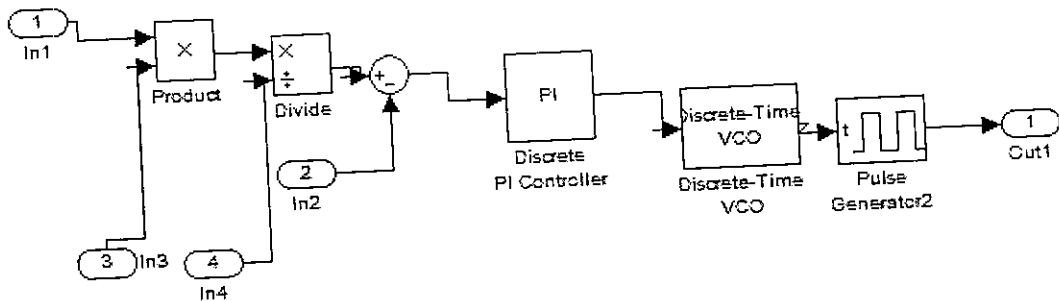


Fig 5.2 MPPT Control block

### 5.2.3 SINGLE PHASE LOAD

The Single-Phase Series RLC Load block implements a Single-phase balanced load. Five different resistive loads connected in parallel, each load have a different resistive values.



Fig 5.3 Resistive Load

## SPECIFICATION

Table 1. Specification

S.NO	DEVICE	RATING
1	Solar panel voltage(maximum)	200V
2	Wind generator voltage(maximum)	200V
3	Lead-Acid Battery	200v,2Ah,50%(SOC)
4	Pi controller	$K_p=0.1, K_i=1$
5	Dc bus voltage	200v
6	Load resistance	100ohm, 100ohm, 10ohm, 50ohm, 10ohm,
7	Carrier frequency	1080Hz
8	Sampling frequency	1KHz
9	<b><u>Boost circuit</u></b>	
	Boost inductor	1H
	Boost Capacitor	10uF



## 5.3 SIMULATION RESULTS

### 5.3.1 LOAD PROFILE

The load profile is shown in Fig 5.4. Here five different loads are connected.

Load current for different time interval is shown in Table 2.

Table 2. Load profile

DURATION	LOAD CURRENT
0S to 80S	30A
80S to 120S	19A
120S to 160S	4A
160S to 190S	3A
190S to 200S	2A

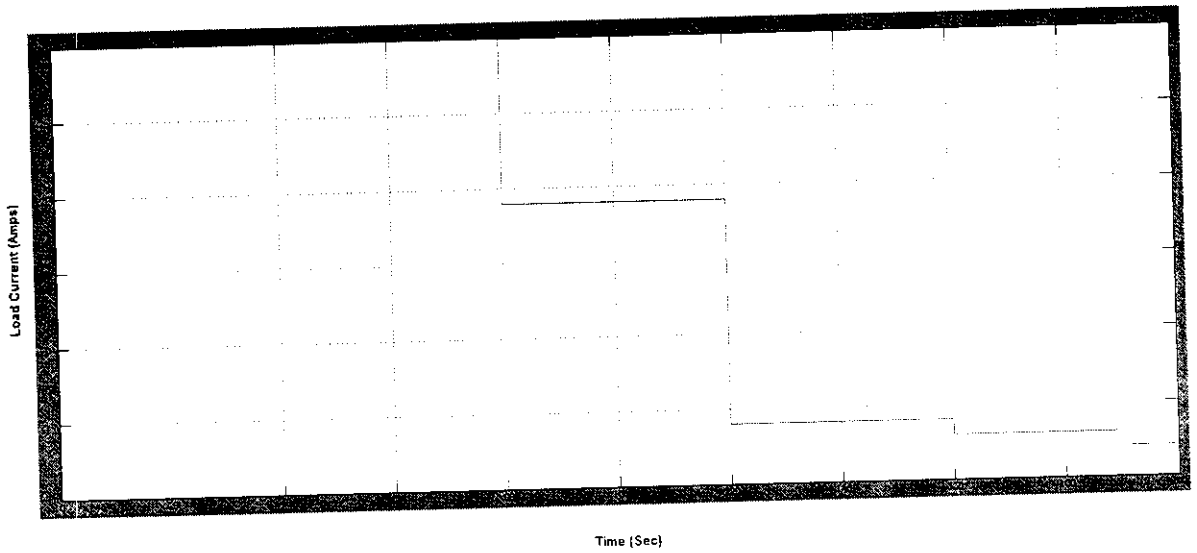


Fig 5.4 Load Profile

### 5.3.2 LOAD CURRENT

The current flows in load is shown in fig 5.5. At starting full load is connected to source. But current from Solar and Wind is low so that controller switches the battery to supply the extra current. So three sources connected to load. After 80s to 120s, total load is 19A. Here also current supplied to load by three sources. After 120s to 160s load is reduced to 4A. this supplied by solar source because that sources is enough to supply. So that wind source is tripped. Similarly 3A and 2A load is supplied by solar only.

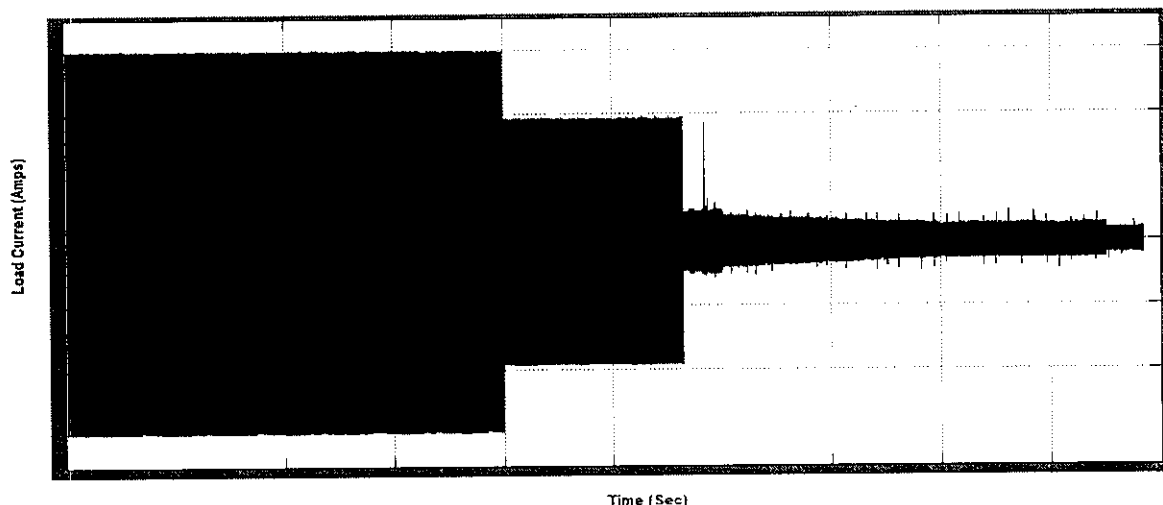


Fig 5.5 Load Current

### 5.3.3 COMPARISION OF LOAD CURRENT WITH LOAD PROFILE

Here load current and load profile is compared and shown in fig 5.6. The line shows the load profile and shaded portion represents the load current. Initially three sources supplies the current that is solar, wind and battery. Initially battery is 40% charged condition. At 115s battery charge condition reaches the 30%, due to low charge battery was tripped. So the particular load also tripped.

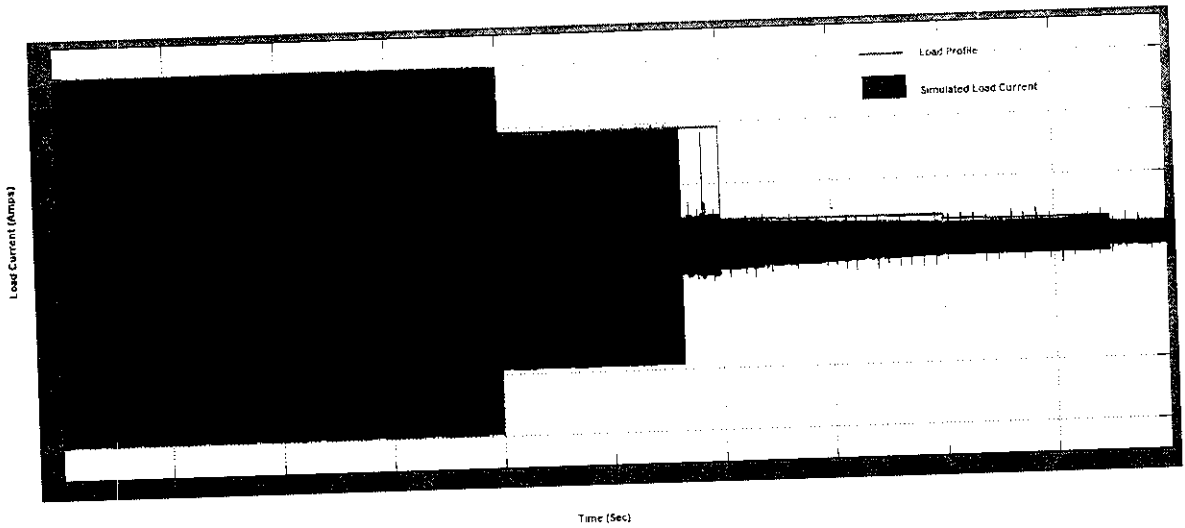


Fig 5.6 Comparison of Load current with Load profile

### 5.3.4 BATTERY STATUS

The battery discharging characteristics is shown in fig 5.7. Initially battery was discharging after 115s battery reaches 30% charge state. So the controller trips the battery.

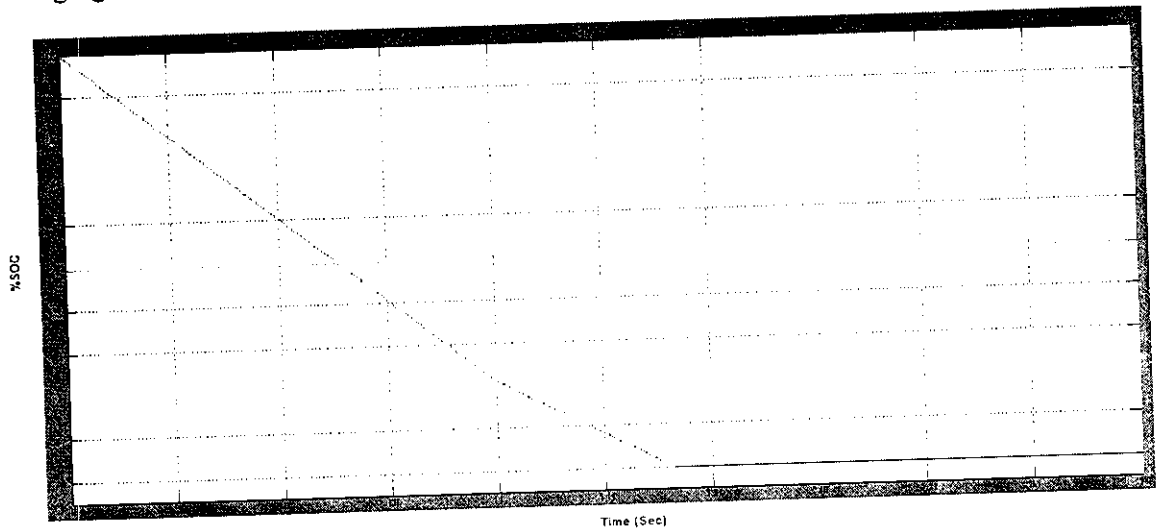


Fig 5.7 Battery SOC Status

---

---

## CHAPTER 6

---

---

## CHAPTER 6

### HARDWARE IMPLEMENTATION OF HYBRID SYSTEM

#### 6.1 BLOCK DIAGRAM OF HYBRID SYSTEM

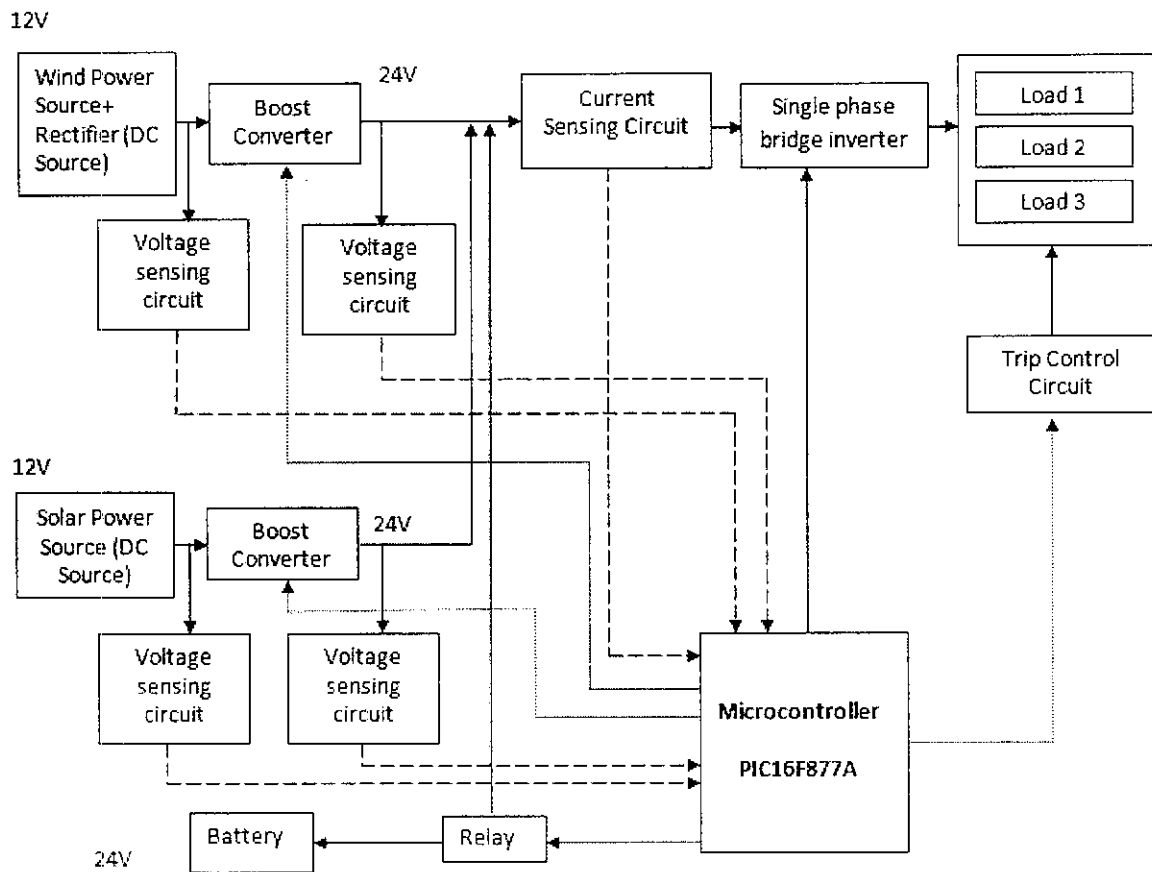


Fig 6.1 Hardware Block diagram

The prototype of the proposed system has single phase step down diode rectifier, single phase three level inverter, soft-switching module and micro controller (PIC16F877A) with 5V power supply. These parts are explained with schematic diagram in following sections.

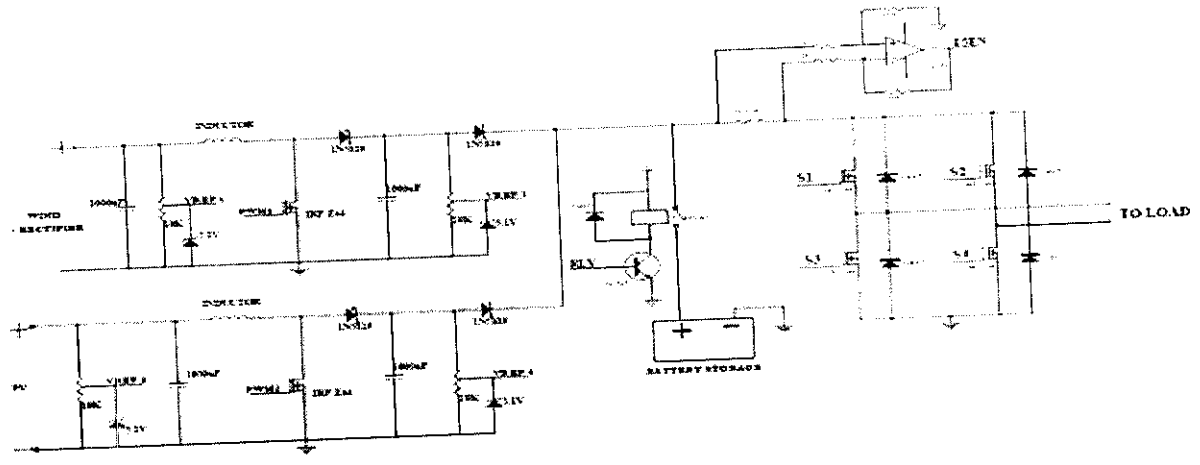


Fig 6.2 Schematic diagram of Hybrid system

### 6.1.1 RECTIFIER PART OF HYBRID SYSTEM

The rectifier block contains a step down transformer, which step downs the input voltage from 220V to 12V. In addition, the step downed voltage is rectified to DC. This is done by uncontrolled single phase diode rectifier. The output of this block is 12V DC. The schematic of rectifier is shown in the fig.6.2.

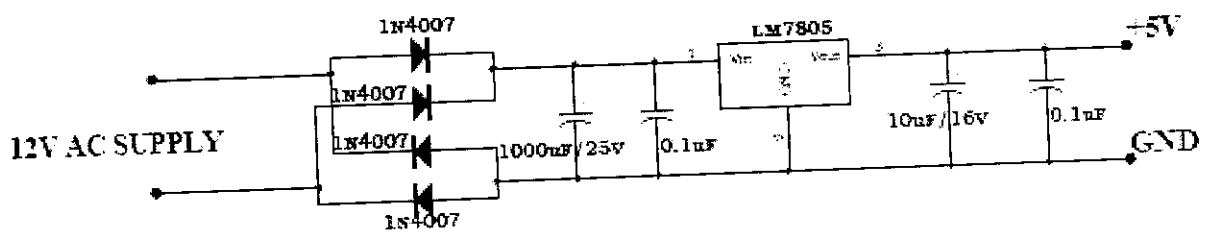


Fig 6.3 Schematic of Power circuit

### 6.1.2 INVERTER PART OF HYBRID SYSTEM

The single phase three level inverter is used in this part. Here four MOSFETs are used in the bridge. These power switches are driven by the gate pulse generated by micro controller (PIC16F877A). The inverter bridge is isolated from the gating circuit by the opto-coupler. The resistive load is connected across the load side of the inverter. The schematic of single phase inverter is shown in the Fig.6.4.

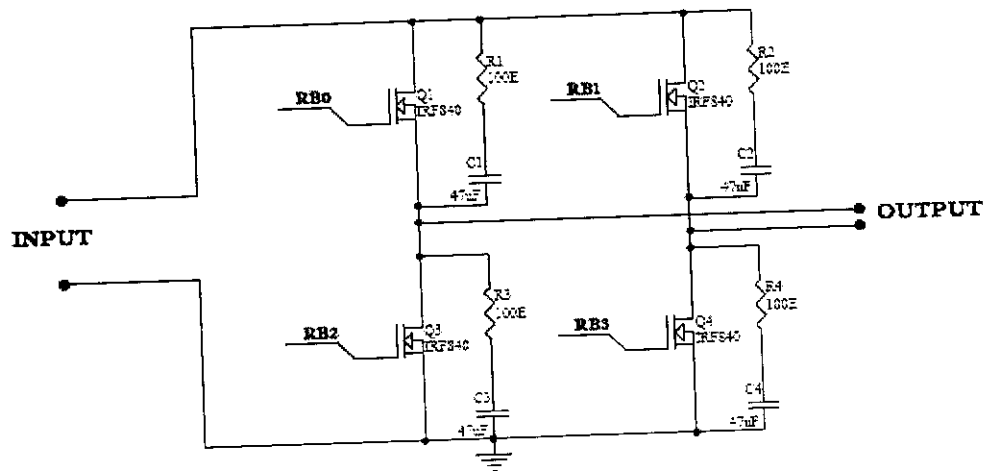


Fig 6.4 Schematic of single phase inverter

#### ADVANTAGES OF MOSFET

- MOSFETs provide much better system reliability.
- MOSFET are fast switching devices permit much higher switching frequencies and there by the efficiency is increased.
- MOSFETs have better temperature stability.
- Overload and peak current handling capacity is high.
- MOSFETS have low leakage current.
- MOSFETs are able to operate in hazardous radiation environments.

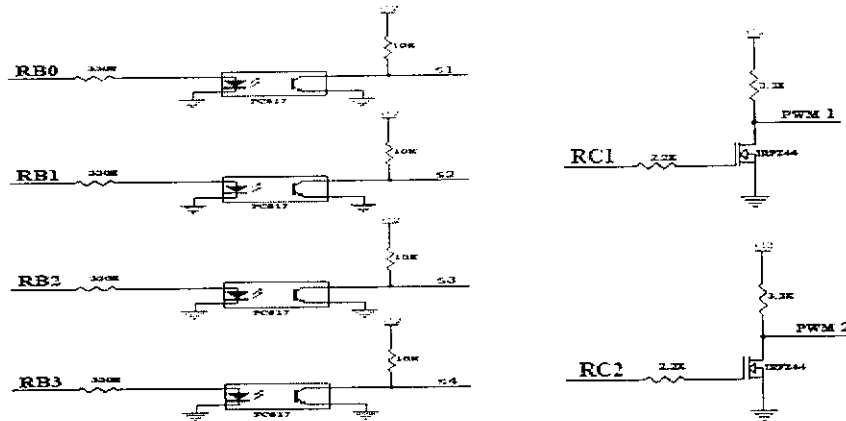


Fig 6.5 Schematic of driving circuit

### 6.1.3 MICROCONTROLLER FOR HYBRID SYSTEM

The gate pulse for the inverter switches and the switches in soft-switching module is generated by PIC16F877A controller. This micro controller circuit works in 5V power supply. So separate step down rectifier unit is made for the controller. The details about PIC16F877A is given in APPENDIX II. This controller is isolated from the main circuits by means of opto-coupler. The schematic of micro controller circuit is shown in Fig.6.6.

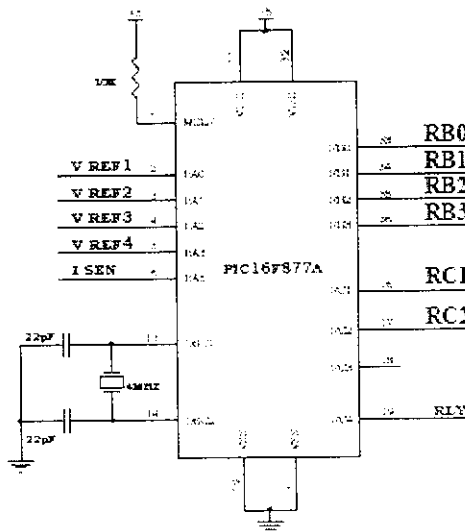


Fig 6.6 Schematic of micro controller circuit



## 6.2 PHOTOGRAPH OF HARDWARE



Fig 6.7 Photo copy of Hardware

The hardware block diagram is shown in Fig 6.7. It has two battery sources for solar, wind with rectifier. Each have a 12V energy and also variable sources. To maintain constant output voltage at dc bus, the boost converter used for both sources. Dc bus voltage is 24V and Battery potential is 24V connected to dc bus. A single phase bridge inverter converts dc to square wave ac signal. Three different types of resistive load connected ac bus. The PIC 16F877A controller controls the power demand. The system is continuously monitored by computer.

## 6.3 HARDWARE RESULTS

### 6.3.1 BATTERY CONDITION



Fig 6.8 Battery charging waveform

### 6.3.2 PWM PULSES

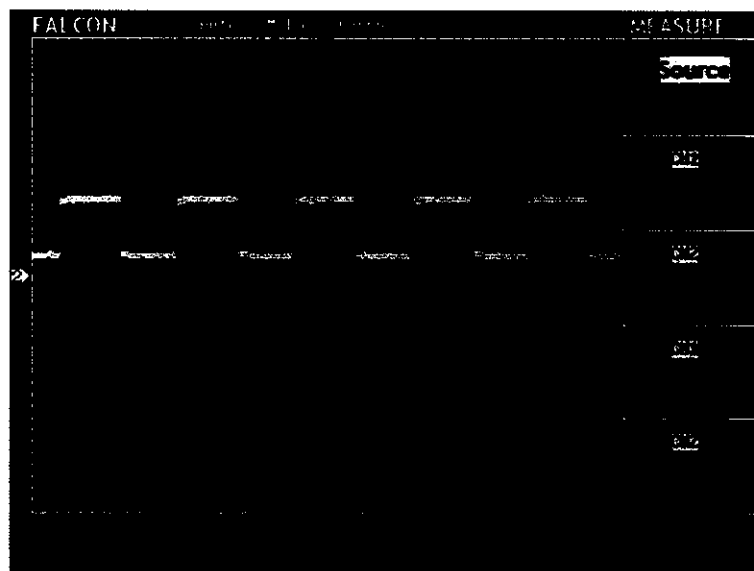


Fig 6.9 PWM Pulse for Boost converter

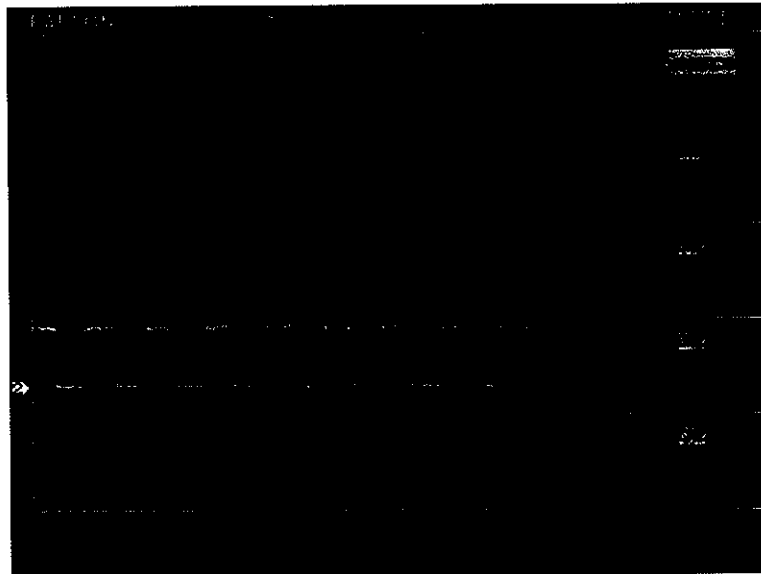


Fig 6.10 PWM Pulse for Inverter

### 6.3.4 AC BUS VOLTAGE

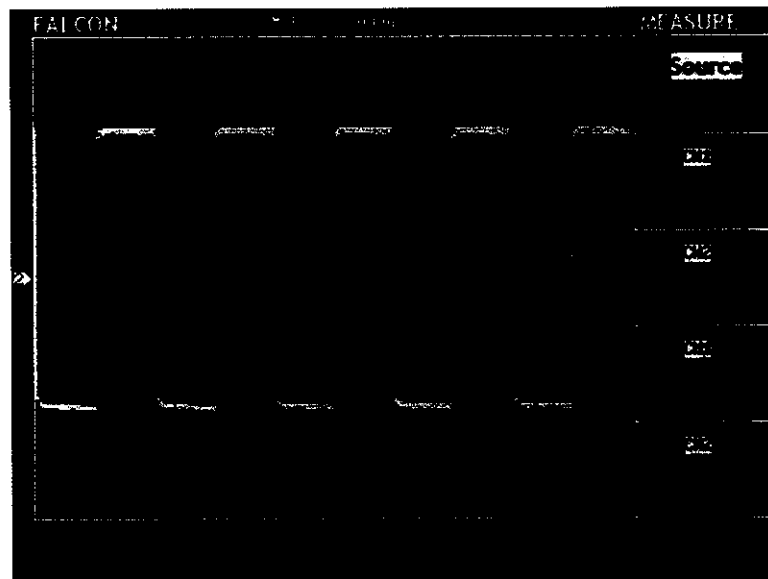


Fig 6.11 AC bus voltage

---

---

## CHAPTER 7

---

---

## CHAPTER 7

### CONCLUSION AND FUTURE SCOPE

#### 7.1 CONCLUSION

This project shows that a simulation for a hybrid PV-wind generator system and Battery connected to the DC bus. The dc voltage is inverted and used for different load. An Optimal controller was designed to meet power demand and MPPT for solar and wind also designed. The different components of the system were modeled and the control strategies for the different parts of the system were proposed. The simulation process illustrated the voltages in the different components of the system with one input conditions of solar radiation, wind speed and temperature. The measurement of voltages are used as a data for smart grid application. By using renewable energy sources the power demand is compensated and environmental is clean by lower usage of fossil fuels.

#### 7.2 FUTURE SCOPE

The system proposed to modify the control strategies and implements more number of renewable energy sources. It can be modify the system optimize and reduced total cost. The data from the sources sent to smart grid controllers. The data can be collected by Smart Meters from houses and industries.

## REFERENCES

- [1] J. A. Gow and C. D. Manning, "Development of a model for photovoltaic arrays suitable for use in simulation studies of solar energy conversion systems," in Proc. 6th Int. Conf. Power Electron. Variable Speed Drives, 1996, pp. 69–74.
- [2] J. Hyvarinen and J. Karila, "New analysis method for crystalline silicon cells," in Proc. 3rd World Conf. Photovoltaic Energy Convers., 2003, vol. 2, pp. 1521–1524.
- [3] M. Veerachary, "PSIM circuit-oriented simulator model for the nonlinear photovoltaic sources," IEEE Trans. Aerosp. Electron. Syst., vol. 42, no. 2, pp. 735–740, Apr. 2006
- [4] F. Lasnier and T. G. Ang, "Photovoltaic Engineering Handbook". New York: Adam Hilger, 1990.
- [5] J. A. Gow and C. D. Manning, "Development of a photovoltaic array model for use in power-electronics simulation studies," *IEE Proc. Elect. Power Appl.*, vol. 146, no. 2, pp. 193–200, 999.
- [6] L. Castañer and S. Silvestre, *Modeling Photovoltaic Systems Using PSpice*. New York: Wiley, 2002.
- [7] A. Guechi and M. Chegaar, "Effects of diffuse spectral illumination on microcrystalline solar cells," *J. Electron Devices*, vol. 5, pp. 116–121, 2007.
- [8] C. Riordan and R. Hulstron, "What is an air mass 1.5 spectrum? [solar cell performance calculations]," in Proc. Conf.
- [9] J. F. Manwell, J. G. McGowan, and A. L. Rogers, *Wind Energy Explained: Theory, Design and Application*, West Sussex, England: John Wiley & Sons, 2002
- [10] S. N. Bhadra, D. Kastha, S. Banerjee, *Wind Electrical Systems*, Oxford, UK: Oxford University Press, 2005.

- [11] I. H. Altas and A. M. Sharaf, "A photovoltaic array simulation model for matlab–simulink GUI environment," in Proc. Int. Conf. Clean Elect.Power (ICCEP), 2007, pp. 341–345
- [12] R. Chedid and S. Rahman, "Unit sizing and control of hybrid wind-solar power systems". IEEE Transactions on energy conversion, Vol.12, N°1, March 1997, pp. 79-85.
- [13]Mahmoud M.M. "On the Storage Batteries Used in Solar Electric Power Systems and Development of an Algorithm for Determining their Ampere-Hour Capacity". Electric Power Systems Research 2004. 71(85-89)
- [14] V. Salas, E. Olias, A. Barrado and A. Lazaro, "Review of the maximum power point tracking algorithms for stand-alone photovoltaic systems", Elsevier, 2005.
- [15] A.M. De Broe, S. Drouilhet and V. Gevorgian, "A peak power tracker for small wind turbines in battery charging applications". IEEE Transactions on energy conversion, Vol. 14, N°4, December 1999, pp. 1630-1635.

## **APPENDIX I**



## OPTIMAL DISPATCH CONTROLLER

```
function [l,s,b] = fcn(si,wi,li,Btsoc)
% This block supports the Embedded MATLAB subset.
% See the help menu for details.
ti=si+wi;%ti means total current
l=0;
b=0;
s=0;
if ti>li
    x=ti-li;
    b=1; %load takes required current and battery CHARGING
    l=1;
    if Btsoc>=0.8
        b=0; %battery should be disconnected(b=0)
    else
        b=1;%charging of battery
        l=1;%load is connected
    end
else if ti<li
    if Btsoc>0.3
        b=1;%connect the battery
        l=1;
        if Btsoc<0.3
```

```
    b=0;%disconnect the battery
    l=0;%Particular load is disconnected
else
    b=1;%connect the battery
    l=1;
end
else
    l=0;%load cannot take current(l=0)
    b=1;
end
else
    b=0;%battery disconnected to load
    l=1;
end
end
end
```

## **APPENDIX II**

# LM2904, LM358/LM358A, LM258/ LM258A

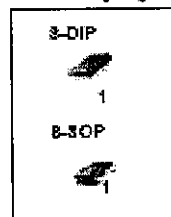
## Dual Operational Amplifier

### Features

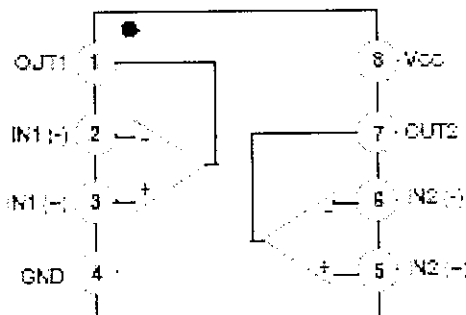
- Internally Frequency Compensated for Unity Gain
- Large DC Voltage Gain: 100dB
- Wide Power Supply Range:  
LM258/LM258A, LM358/LM358A: 3V-32V (or  $\pm 1.5V$  ~ 16V)  
LM2904: 3V-26V (or  $\pm 1.5V$  ~ 13V)
- Input Common Mode Voltage Range Includes Ground
- Large Output Voltage Swing: 0VDC to  $V_{CC} - 1.5VDC$
- Power Drain Suitable for Battery Operation

### Description

The LM2904, LM358/LM358A, LM258/LM258A consist of two independent, high gain, internally frequency compensated operational amplifiers which were designed specifically to operate from a single power supply over a wide range of voltage. Operation from split power supplies is also possible and the low power supply current drain is independent of the magnitude of the positive supply voltage. Application areas include transducer amplifier, DC gain blocks and all the conventional OP-AMP circuits which now can be easily implemented in single power supply systems.

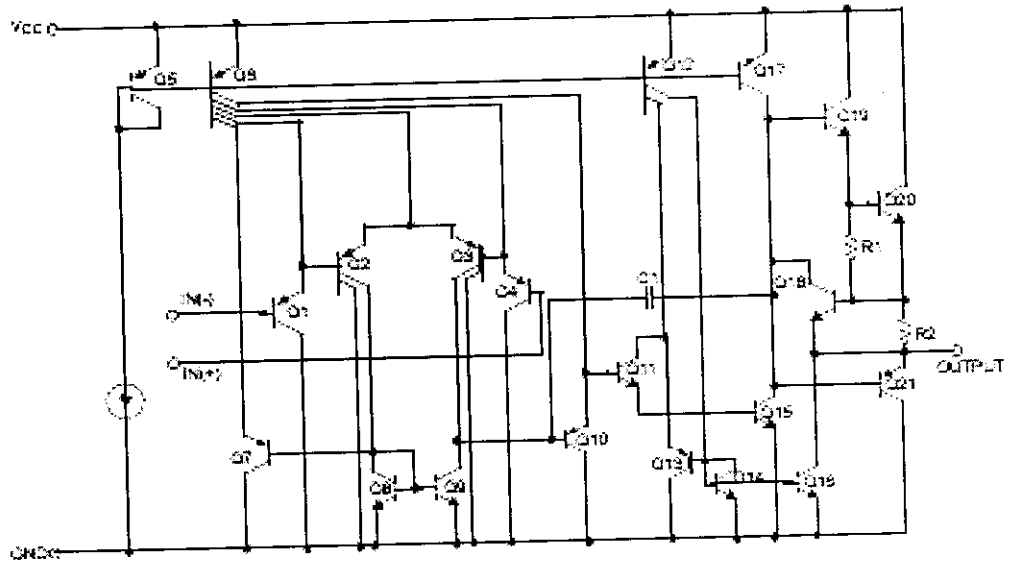


### Internal Block Diagram



### Schematic Diagram

(One section only)



### Absolute Maximum Ratings

Parameter	Symbol	LM258/LM258A	LM358/LM358A	LM2504	Unit
Supply Voltage	V <sub>CC</sub>	±15 or 32	±15 or 32	±15 or 25	V
Differential Input Voltage	V <sub>I(DIFF)</sub>	32	32	25	V
Input Voltage	V <sub>I</sub>	-0.3 to -32	-0.3 to +32	-0.3 to +26	V
Output Short Circuit to GND (V <sub>CC</sub> ±15V, T <sub>A</sub> = 25°C, One Amp)	-	Continuous	Continuous	Continuous	-
Operating Temperature Range	T <sub>OPR</sub>	-25 ~ +85	0 ~ +70	-40 ~ +85	°C
Storage Temperature Range	T <sub>STG</sub>	-65 ~ +150	-65 ~ +150	-65 ~ +150	°C

## Electrical Characteristics

(V<sub>CC</sub> = 5.0V, V<sub>EE</sub> = GND, T<sub>A</sub> = 25°C, unless otherwise specified)

Parameter	Symbol	Conditions	LM258			LM358			LM2904			Unit
			Min.	Typ.	Max.	Min.	Typ.	Max.	Min.	Typ.	Max.	
Input Offset Voltage	V <sub>IO</sub>	V <sub>CM</sub> = 0V to V <sub>CC</sub> -1.5V V <sub>OLP</sub> = 1.4V, R <sub>S</sub> = 0Ω	-	2.9	5.0	-	2.9	7.0	-	2.9	7.0	mV
Input Offset Current	I <sub>IO</sub>	-	-	3	30	-	5	50	-	5	50	nA
Input Bias Current	I <sub>BIAS</sub>	-	-	45	150	-	45	250	-	45	250	nA
Input Voltage Range	V <sub>IKR</sub>	V <sub>CC</sub> = 30V (LM2904, V <sub>CC</sub> = 25V)	0	-	V <sub>CC</sub> -1.5	0	-	V <sub>CC</sub> -1.5	0	-	V <sub>CC</sub> -1.5	V
Supply Current	I <sub>CC</sub>	R <sub>L</sub> = ∞, V <sub>CC</sub> = 30V (LM2904, V <sub>CC</sub> = 25V)	-	0.8	2.0	-	0.8	2.0	-	0.8	2.0	mA
		R <sub>L</sub> = ∞, V <sub>CC</sub> = 5V	-	0.5	1.2	-	0.5	1.2	-	0.5	1.2	mA
Large Signal Voltage Gain	G <sub>v</sub>	V <sub>CC</sub> = 15V, R <sub>L</sub> = 2kΩ V <sub>OLP</sub> = 1V to 11V	50	100	-	25	100	-	25	100	-	V/mV
Output Voltage Swing	V <sub>O(H)</sub>	V <sub>CC</sub> = 30V, R <sub>L</sub> = 2kΩ	25	-	-	25	-	-	22	-	-	V
		(V <sub>CC</sub> = 25V for LM2904), R <sub>L</sub> = 10kΩ	27	28	-	27	28	-	23	24	-	V
	V <sub>O(L)</sub>	V <sub>CC</sub> = 5V, R <sub>L</sub> = 10kΩ	-	5	20	-	5	20	-	5	20	mV
Common-Mode Rejection Ratio	CMRR	-	70	85	-	65	80	-	50	60	-	dB
Power Supply Rejection Ratio	PSRR	-	65	100	-	65	100	-	50	100	-	dB
Channel Separation	CS	f = 1kHz to 20kHz (Note 1)	-	120	-	-	120	-	-	120	-	dB
Short Circuit to GND	I <sub>SC</sub>	-	-	40	60	-	40	60	-	40	60	mA
Output Current	I <sub>SOURCE</sub>	V <sub>IN</sub> = 1V, V <sub>IN</sub> = 0V, V <sub>CC</sub> = 15V, V <sub>OLP</sub> = 2V	20	30	-	20	30	-	20	30	-	mA
		V <sub>IN</sub> = 0V, V <sub>IN</sub> = 1V, V <sub>CC</sub> = 15V, V <sub>OLP</sub> = 2V	10	15	-	10	15	-	10	15	-	mA
	I <sub>SINK</sub>	V <sub>IN</sub> = 0V, V <sub>IN</sub> = -1V, V <sub>CC</sub> = 15V, V <sub>OLP</sub> = 200mV	12	100	-	12	100	-	-	-	-	μA
Differential Input Voltage	V <sub>I(DIFF)</sub>	-	-	-	V <sub>CC</sub>	-	-	V <sub>CC</sub>	-	-	V <sub>CC</sub>	V

## Notes:

1. This parameter, although guaranteed, is not 100% tested in production.

# MC78XX/LM78XX/MC78XXA

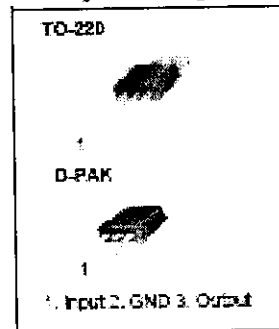
## 3-Terminal 1A Positive Voltage Regulator

### Features

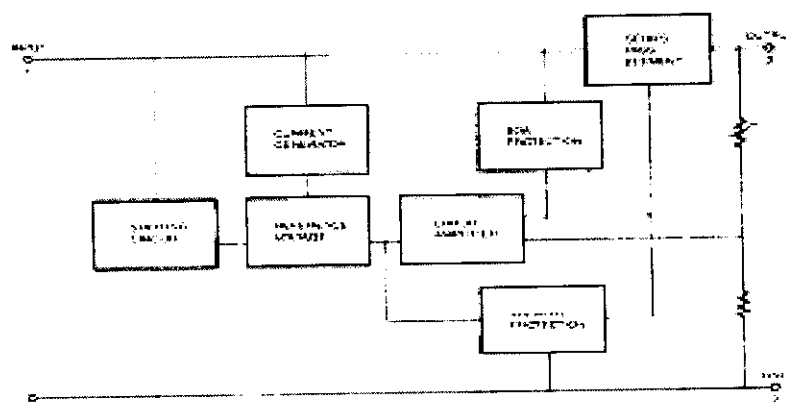
- Output Current up to 1A
- Output Voltages of 5, 6, 8, 9, 10, 12, 15, 18, 24V
- Thermal Overload Protection
- Short Circuit Protection
- Output Transistor Safe Operating Area Protection

### Description

The MC78XX/LM78XX/MC78XXA series of three terminal positive regulators are available in the TO-220/D-PAK package and with several fixed output voltages, making them useful in a wide range of applications. Each type employs internal current limiting, thermal shut down and safe operating area protection, making it essentially indestructible. If adequate heat sinking is provided, they can deliver over 1A output current. Although designed primarily as fixed voltage regulators, these devices can be used with external components to obtain adjustable voltages and currents.



### Internal Block Diagram



## Absolute Maximum Ratings

Parameter	Symbol	Value	Unit
Input Voltage (for $V_O = 5V$ to $18V$ ) (for $V_O = 24V$ )	$V_I$	35	V
	$V_{I1}$	42	V
Thermal Resistance Junction-Cases (TO-220)	$R_{\theta JC}$	5	$^{\circ}C/W$
Thermal Resistance Junction-Air (TO-220)	$R_{\theta JA}$	55	$^{\circ}C/W$
Operating Temperature Range	$T_{OPR}$	0 ~ +125	$^{\circ}C$
Storage Temperature Range	$T_{STG}$	-65 ~ +150	$^{\circ}C$

## Electrical Characteristics (MC7805/LM7805)

(Refer to test circuit,  $0^{\circ}C < T_J < 125^{\circ}C$ ,  $I_O = 500mA$ ,  $V_I = 10V$ ,  $C_s = 0.33\mu F$ ,  $C_O = 0.1\mu F$ , unless otherwise specified)

Parameter	Symbol	Conditions	MC7805/LM7805			Unit	
			Min.	Typ.	Max.		
Output Voltage	$V_O$	$T_J = +25^{\circ}C$	4.8	5.0	5.2	V	
		$5.0mA < I_O < 1.0A$ , $P_D \leq 15W$ $V_I = 7V$ to $20V$	4.75	5.0	5.25		
Line Regulation (Note 1)	Regline	$T_J = +25^{\circ}C$	$V_O = 7V$ to $25V$	-	4.0	100	mV
			$V_I = 8V$ to $12V$	-	1.5	50	
Load Regulation (Note 1)	Regload	$T_J = +25^{\circ}C$	$I_O = 5.0mA$ to $1.5A$	-	9	100	mV
			$I_O = 250mA$ to $750mA$	-	4	50	
Quiescent Current	$I_Q$	$T_J = +25^{\circ}C$	-	5.0	8.0	mA	
Quiescent Current Change	$\Delta I_Q$	$I_O = 5mA$ to $1.0A$	-	0.03	0.5	mA	
		$V_I = 7V$ to $25V$	-	0.3	1.3		
Output Voltage Drift	$\Delta V_O/\Delta T$	$I_O = 5mA$	-	-0.5	-	mV/ $^{\circ}C$	
Output Noise Voltage	$V_N$	$f = 10Hz$ to $100kHz$ , $T_A = +25^{\circ}C$	-	42	-	$\mu V/V_O$	
Ripple Rejection	RR	$f = 120Hz$ $V_O = 5V$ to $15V$	62	73	-	dB	
Dropout Voltage	$V_{DROPP}$	$I_O = 1A$ , $T_J = +25^{\circ}C$	-	2	-	V	
Output Resistance	$r_O$	$f = 1kHz$	-	15	-	m $\Omega$	
Short Circuit Current	$I_{SC}$	$V_I = 35V$ , $T_A = +25^{\circ}C$	-	230	-	mA	
Peak Current	$I_{PK}$	$T_J = +25^{\circ}C$	-	2.2	-	A	

## Notes:

1. Load and line regulation are specified at constant junction temperature. Changes in  $V_O$  due to heating effects must be taken into account separately. Pulse testing with low duty is used.



# 1N4001 - 1N4007

## Features

- Low forward voltage drop.
- High surge current capability.



DO-41

COLOR BAND DENOTES CATHODE

## General Purpose Rectifiers (Glass Passivated)

### Absolute Maximum Ratings\* T<sub>A</sub> = 25°C unless otherwise noted

Symbol	Parameter	Value							Units
		4001	4002	4003	4004	4005	4006	4007	
V <sub>RRM</sub>	Peak Repetitive Reverse Voltage	50	100	200	400	600	800	1000	V
I <sub>F(AV)</sub>	Average Rectified Forward Current, 375 μ lead length @ T <sub>A</sub> = 75°C	1.0							A
I <sub>FSM</sub>	Non-repetitive Peak Forward Surge Current 8.3 ms Single Half-Sine-Wave	30							A
T <sub>stg</sub>	Storage Temperature Range	-55 to +175							°C
T <sub>J</sub>	Operating Junction Temperature	-55 to +175							°C

\*These ratings are limiting values above which the serviceability of any semiconductor device may be impaired.

### Thermal Characteristics

Symbol	Parameter	Value	Units
P <sub>D</sub>	Power Dissipation	3.0	W
R <sub>θJA</sub>	Thermal Resistance, Junction to Ambient	50	°C/W

### Electrical Characteristics T<sub>A</sub> = 25°C unless otherwise noted

Symbol	Parameter	Device							Units
		4001	4002	4003	4004	4005	4006	4007	
V <sub>F</sub>	Forward Voltage @ 1.0 A	1.1							V
I <sub>rr</sub>	Maximum Full Load Reverse Current, Full Cycle T <sub>A</sub> = 75°C	30							μA
I <sub>r</sub>	Reverse Current @ rated V <sub>R</sub> T <sub>A</sub> = 25°C T <sub>A</sub> = 100°C	5.0 500							μA μA
C <sub>T</sub>	Total Capacitance V <sub>R</sub> = 4.0 V, f = 1.0 MHz	15							pF



1N581x

LOW DROP POWER SCHOTTKY RECTIFIER

MAIN PRODUCTS CHARACTERISTICS

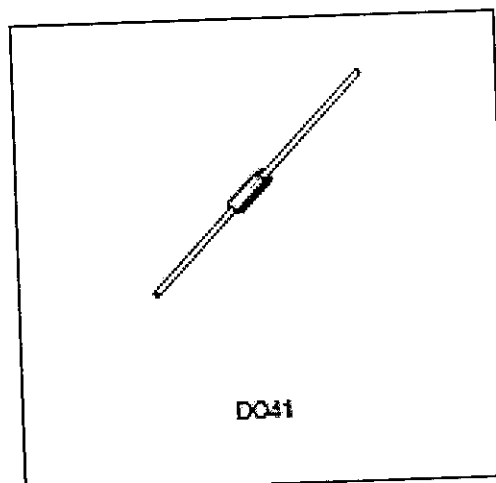
$I_{F(AV)}$	1 A
$V_{RRM}$	40 V
$T_j$	150°C
$V_f$ (max)	0.45 V

FEATURES AND BENEFITS

- VERY SMALL CONDUCTION LOSSES
- NEGLIGIBLE SWITCHING LOSSES
- EXTREMELY FAST SWITCHING
- LOW FORWARD VOLTAGE DROP
- AVALANCHE CAPABILITY SPECIFIED

DESCRIPTION

Axial Power Schottky rectifier suited for Switch Mode Power Supplies and high frequency DC to DC converters. Packaged in DO41 these devices are intended for use in low voltage, high frequency inverters, free wheeling, polarity protection and small battery chargers.

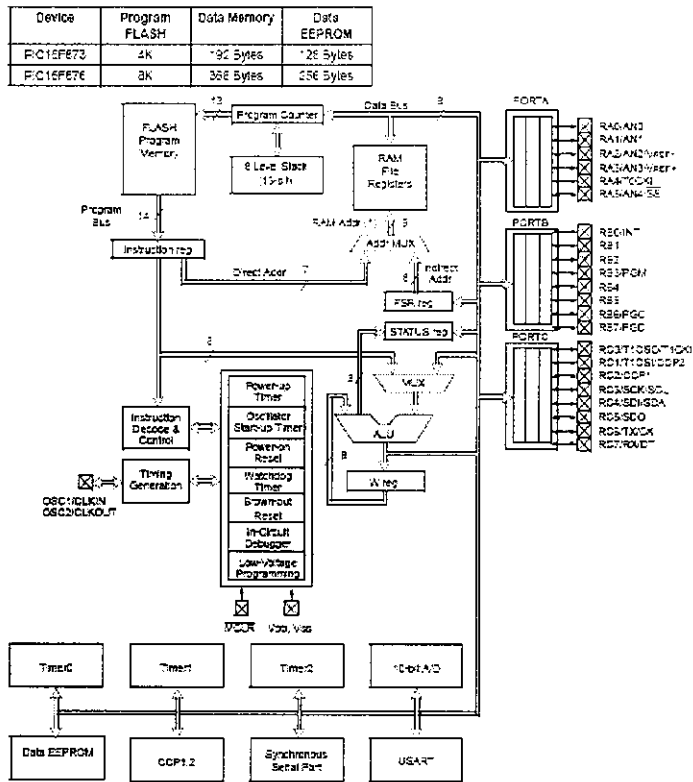


ABSOLUTE RATINGS (limiting values)

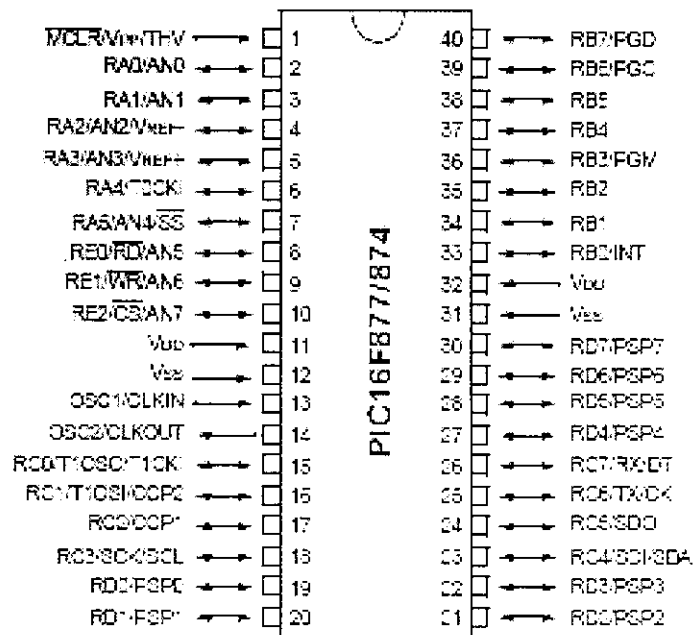
Symbol	Parameter	Value			Unit
		1N5817	1N5818	1N5819	
$V_{RRM}$	Repetitive peak reverse voltage	20	30	25	V
$I_{F(RMS)}$	RMS forward current	10			A
$I_{F(AV)}$	Average forward current	1			A
$I_{FSM}$	Surge non repetitive forward current	25			A
$P_{AVM}$	Repetitive peak avalanche power	1200	1200	900	W
$T_{stg}$	Storage temperature range	-55 to +150			°C
$T_j$	Maximum operating junction temperature	150			°C
$dV/dt$	Critical rate of rise of reverse voltage	10000			V/μs

$\theta_{j-c} = \frac{P_{AVM}}{dT_j} < \frac{1}{R_{th(j-c)} - \theta}$  thermal runaway condition for a diode on its own heatsink

# ARCHITECTURE OF PIC16F877A



## Pin Configuration of PIC16F877A



## TIMER 0 CONTROL REGISTER:

R/W-1	R/W-1	R/W-1	R/W-1	R/W-1	R/W-1	R/W-1	R/W-1
RBPV	INTEDG	T0CS	T0SE	PSA	PS2	PS1	PS0
bit 7							bit 0

bit 7: **RBPV**

bit 6: **INTEDG**

bit 5: **T0CS**: TMR0 Clock Source Select bit

1 = Transition on T0CKI pin

0 = Internal instruction cycle clock (CLKOUT)

bit 4: **T0SE**: TMR0 Source Edge Select bit

1 = Increment on high-to-low transition on T0CKI pin

0 = Increment on low-to-high transition on T0CKI pin

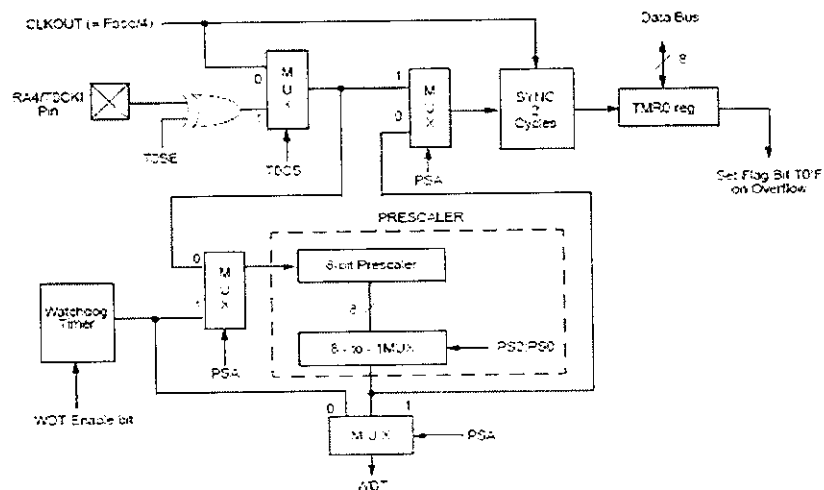
bit 3: **PSA**: Prescaler Assignment bit

1 = Prescaler is assigned to the WDT

0 = Prescaler is assigned to the Timer0 module

bit 2-0: **PS2 PS1 PS0**: Prescaler Rate Select bits

## TIMER 0 BLOCK DIAGRAM:



## TIMER 1 CONTROL REGISTER:

U-0	U-0	R/W-0	R/W-0	R/W-0	R/W-0	R/W-0	R/W-0	
—	—	T1CKPS1	T1CKPS0	T1OSCEN	T1SYNC	TMR1CS	TMR1CN	
bit7								bit0

bit 7-6: **Unimplemented:** Read as '0'

bit 5-4: **T1CKPS1:T1CKPS0:** Timer1 Input Clock Prescale Select bits

11 = 1:8 Prescale value

10 = 1:4 Prescale value

01 = 1:2 Prescale value

00 = 1:1 Prescale value

bit 3: **T1OSCEN:** Timer1 Oscillator Enable Control bit

1 = Oscillator is enabled

0 = Oscillator is shut off (The oscillator inverter is turned off to eliminate power drain)

bit 2: **T1SYNC:** Timer1 External Clock Input Synchronization Control bit

**TMR1CS = 1**

1 = Do not synchronize external clock input

0 = Synchronize external clock input

**TMR1CS = 0**

This bit is ignored. Timer1 uses the internal clock when **TMR1CS = 0**.

bit 1: **TMR1CS:** Timer1 Clock Source Select bit

1 = External clock from pin RC0/T1OSO/T1CKI (on the rising edge)

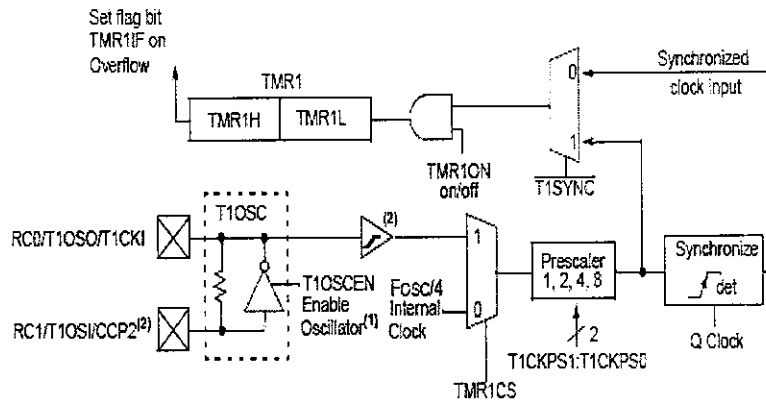
0 = Internal clock (FOSC/4)

bit 0: **TMR1ON**: Timer1 On bit

1 = Enables Timer1

0 = Stops Timer1

**TIMER 1 BLOCK DIAGRAM:**



**TIMER 2 CONTROL REGISTER:**

U-0	R/W-0	R/W-0	R/W-0	R/W-0	R/W-0	R/W-0	R/W-0
—	TOUTPS3	TOUTPS2	TOUTPS1	TOUTPS0	TMR2ON	T2CKPS1	T2CKPS0
bit7							bit0

bit 7: **Unimplemented**: Read as '0'

bit 6-3: **TOUTPS3:TOUTPS0**: Timer2 Output Postscale Select bits

0000 = 1:1 Postscale

0001 = 1:2 Postscale

0010 = 1:3 Postscale

1111 = 1:16 Postscale

bit 2: **TMR2ON**: Timer2 On bit

1 = Timer2 is on

0 = Timer2 is off

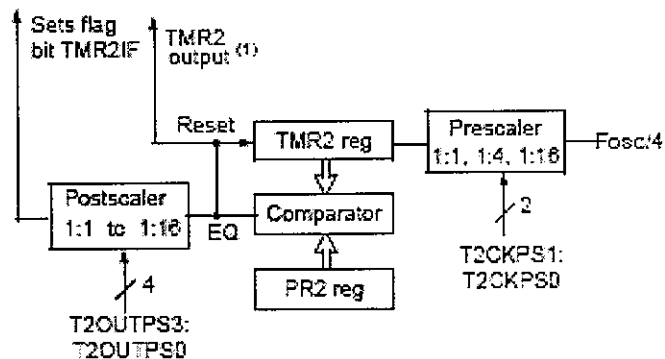
bit 1-0: **T2CKPS1:T2CKPS0**: Timer2 Clock Prescale Select bits

00 = Prescaler is 1

01 = Prescaler is 4

1x = Prescaler is 16

### TIMER2 BLOCK DIAGRAM:



### CCP1CON REGISTER/CCP2CON REGISTER:

U-0	U-0	R/W-0	R/W-0	R/W-0	R/W-0	R/W-0	R/W-0
—	—	CCPxX	CCPxY	CCPxM3	CCPxM2	CCPxM1	CCPxM0
bit7							bit0

bit 7-6: **Unimplemented**: Read as '0'

bit 5-4: **CCPxX :CCPxY**: PWM Least Significant bits

Capture Mode: Unused

Compare Mode: Unused

PWM Mode: These bits are the two LSB s of the PWM duty cycle. The eight MSB s are found in CCPRxL.

bit 3-0: **CCPxM3:CCPxM0**: CCPx Mode Select bits

0000 = Capture/Compare/PWM off (resets CCPx module)

0100 = Capture mode, every falling edge

0101 = Capture mode, every rising edge

0110 = Capture mode, every 4th rising edge

0111 = Capture mode, every 16th rising edge

1000 = Compare mode, set output on match (CCPxIF bit is set)

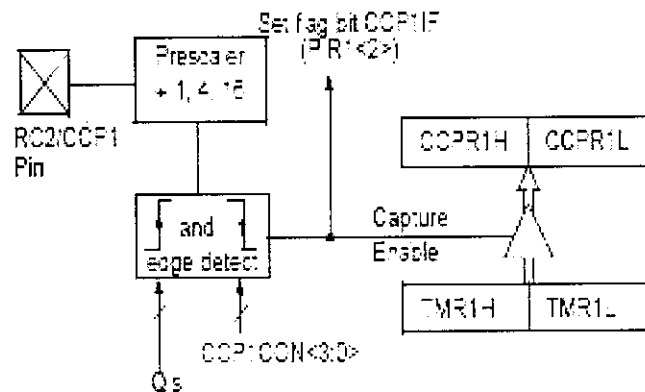
1001 = Compare mode, clear output on match (CCPxIF bit is set)

1010 = Compare mode, generate software interrupt on match (CCPxIF bit is set, CCPx pin is unaffected)

1011 = Compare mode, trigger special event (CCPxIF bit is set, CCPx pin is unaffected); CCP1 resets TMR1; CCP2 resets TMR1 and starts an A/D conversion (if A/D module is enabled)

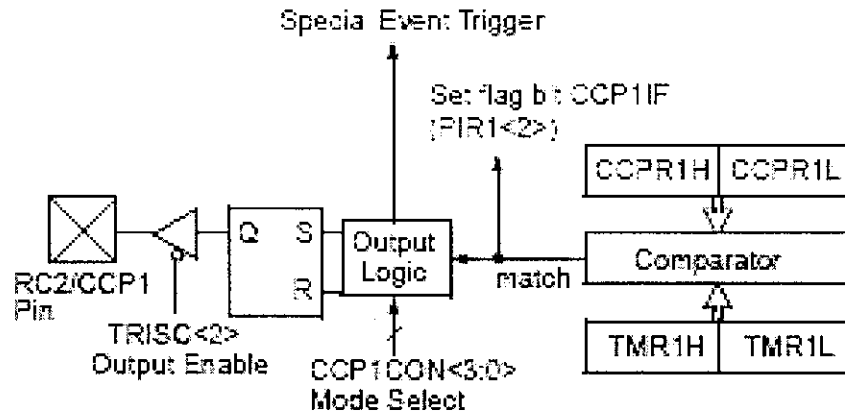
11xx = PWM mode

### CAPTURE MODE OPERATION BLOCK DIAGRAM:





### COMPARE MODE OPERATION BLOCK DIAGRAM:



**N-channel enhancement mode  
TrenchMOS™ transistor**

**IRFZ44N**

**GENERAL DESCRIPTION**

N-channel enhancement mode standard level field-effect power transistor in a plastic envelope using 'trench' technology. The device features very low on-state resistance and has integral zener diodes giving ESD protection up to 2kV. It is intended for use in switched mode power supplies and general purpose switching applications.

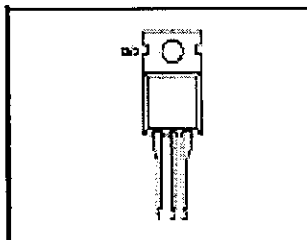
**QUICK REFERENCE DATA**

SYMBOL	PARAMETER	MAX.	UNIT
$V_{DS}$	Drain-source voltage	55	V
$I_D$	Drain current (DC)	49	A
$P_{tot}$	Total power dissipation	110	W
$T_j$	Junction temperature	175	°C
$R_{DS(on)}$	Drain-source on-state resistance $V_{GS} = 10\text{ V}$	22	mΩ

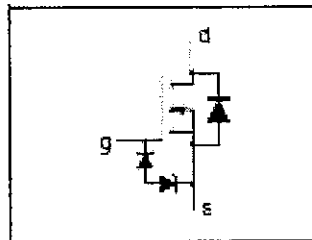
**PINNING - TO220AB**

PIN	DESCRIPTION
1	gate
2	drain
3	source
tab	drain

**PIN CONFIGURATION**



**SYMBOL**



**LIMITING VALUES**

Limiting values in accordance with the Absolute Maximum System (IEC 134)

SYMBOL	PARAMETER	CONDITIONS	MIN.	MAX.	UNIT
$V_{DS}$	Drain-source voltage	-	-	55	V
$V_{GS}$	Drain-gate voltage	$R_{GS} = 20\text{ k}\Omega$	-	55	V
$V_{GS}$	Gate-source voltage	-	-	20	V
$I_D$	Drain current (DC)	$T_{j,c} = 25\text{ }^\circ\text{C}$	-	49	A
$I_D$	Drain current (DC)	$T_{j,c} = 100\text{ }^\circ\text{C}$	-	35	A
$I_{DM}$	Drain current (pulse peak value)	$T_{j,c} = 25\text{ }^\circ\text{C}$	-	162	A
$P_{tot}$	Total power dissipation	$T_{j,c} = 25\text{ }^\circ\text{C}$	-	112	W
$T_{stg}, T_j$	Storage & operating temperature	-	-55	175	°C

**ESD LIMITING VALUE**

SYMBOL	PARAMETER	CONDITIONS	MIN.	MAX.	UNIT
$V_{ESD}$	Electrostatic discharge capacitor voltage, all pins	Human body model (100 pF, 1.5 kΩ)	-	2	kV

**THERMAL RESISTANCES**

SYMBOL	PARAMETER	CONDITIONS	TYP.	MAX.	UNIT
$R_{th(j-c)}$	Thermal resistance (junction to mounting base)	-	-	1.4	°C/W
$R_{th(j-a)}$	Thermal resistance (junction to ambient)	in free air	60	-	°C/W

N-channel enhancement mode  
TrenchMOS™ transistor

IRFZ44N

## STATIC CHARACTERISTICS

T = 25°C unless otherwise specified

SYMBOL	PARAMETER	CONDITIONS	MIN.	TYP.	MAX.	UNIT
$V_{(BR)DSS}$	Drain-source breakdown voltage	$V_{GS} = 0\text{ V}; I_D = 0.25\text{ mA}; T = -55^\circ\text{C}$	55	-	-	V
$V_{GS(th)}$	Gate threshold voltage	$V_{GS} = V_{DS}; I_D = 1\text{ mA}; T = 175^\circ\text{C}$	2.0	3.0	4.0	V
$I_{DSS}$	Zero gate voltage drain current	$V_{GS} = 55\text{ V}; V_{DS} = 0\text{ V}; T = 175^\circ\text{C}$	-	0.05	12	$\mu\text{A}$
$I_{SS}$	Gate source leakage current	$V_{GS} = \pm 15\text{ V}; V_{DS} = 0\text{ V}; T = 175^\circ\text{C}$	-	0.04	1	$\mu\text{A}$
$\frac{\Delta V_{GS(on)}}{R_{DS(on)}}$	Gate source breakdown voltage	$I_D = \pm 1\text{ mA}; V_{DS} = 10\text{ V}; I_D = 25\text{ A}; T = 175^\circ\text{C}$	15	15	22	mV
$R_{DS(on)}$	Drain-source on-state resistance		-	-	42	m $\Omega$

## DYNAMIC CHARACTERISTICS

T<sub>case</sub> = 25°C unless otherwise specified

SYMBOL	PARAMETER	CONDITIONS	MIN.	TYP.	MAX.	UNIT
$g_m$	Forward transconductance	$V_{GS} = 25\text{ V}; I_D = 25\text{ A}$	5	-	-	S
$C_{iE}$	Input capacitance	$V_{GS} = 0\text{ V}; V_{DS} = 25\text{ V}; f = 1\text{ MHz}$	-	1350	1800	pF
$C_{oE}$	Output capacitance		-	330	400	pF
$C_{fE}$	Feedback capacitance		-	15E	21E	pF
$Q_{gT}$	Total gate charge	$V_{GS} = 44\text{ V}; I_D = 50\text{ A}; V_{DS} = 12\text{ V}$	-	-	62	nC
$Q_{gS}$	Gate-source charge		-	-	1E	nC
$Q_{gD}$	Gate-drain (Miller) charge		-	-	2E	nC
$t_{d(on)}$	Turn-on delay time	$V_{GS} = 30\text{ V}; I_D = 25\text{ A}; V_{DS} = 10\text{ V}; R_{\theta Jc} = 10\text{ }^\circ\text{C/W}$	-	1E	2E	ns
$t_{r(on)}$	Turn-on rise time		-	5E	7E	ns
$t_{d(off)}$	Turn-off delay time		-	4E	5E	ns
$t_{f(off)}$	Turn-off fall time		-	3E	4E	ns
$L_{intD}$	Internal drain inductance	Measured from contact screw on tab to centre of die	-	3.5	-	nH
$L_{intS}$	Internal drain inductance	Measured from drain lead 5 mm from package to centre of die	-	4.5	-	nH
$L_{intG}$	Internal source inductance	Measured from source lead 5 mm from package to source bond pad	-	7.5	-	nH

## REVERSE DIODE LIMITING VALUES AND CHARACTERISTICS

T = 25°C unless otherwise specified

SYMBOL	PARAMETER	CONDITIONS	MIN.	TYP.	MAX.	UNIT
$I_{RS}$	Continuous reverse drain current		-	-	40	A
$I_{RSM}$	Pulsed reverse drain current		-	-	150	A
$V_{DF}$	Diode forward voltage	$I = 25\text{ A}; V_{GS} = 0\text{ V}$ $I = 40\text{ A}; V_{GS} = 0\text{ V}$	-	0.9E	1.2	V
$t_{rr}$	Reverse recovery time	$I = 40\text{ A}; -dI/dt = 100\text{ A}/\mu\text{s}; V_{GS} = -10\text{ V}; V_{DS} = 30\text{ V}$	-	27	-	ns
$Q_{rr}$	Reverse recovery charge		-	0.15	-	nC

## APPENDIX III

## PIC CONTROLLER PROGRAM

```
#include<pic.h>
__CONFIG(0X20E4);
__CONFIG(0X3FFF);
#define S1 RB0
#define S2 RB1
#define S3 RB2
#define S4 RB3
#define SW RB5
unsigned int REFF1,INPUT1,REFF2,INPUT2;
unsigned char count;
delay(void);
delay1(void);
void main()
{
    TRISC=0;
    PORTC=0;
    TRISB=0;
    PORTB=0;
    TRISA=0XFF;
    RC2=1;
    ANSEL=0X0F;
    ANSELH=0;
    ADCON1=0X80;
```

```

PR2=99;
T2CON=0X04;
CCP1CON=0X0C;
CCPR1L=75;
CCP2CON=0X0C;
CCPR2L=75;
T1CON=0X01;
TMR1L=0XF0;
TMR1H=0XD8;
GIE=PEIE=TMR1IE=1;
while(1)
{

```

```

/***** ADC SCAN *****/

```

```

    ADCON0=0X81;
    delay();
    GODONE=1;
    while(GODONE);
    REFF1=(ADRESH*256)+ADRESL;
    ADCON0=0X85;
    delay();
    GODONE=1;
    while(GODONE);
    INPUT1=(ADRESH*256)+ADRESL;

    ADCON0=0X89;

```

```

delay();

GODONE=1;

while(GODONE);

REFF2=(ADRESH*256)+ADRESL;

ADCON0=0X8D;

delay();

GODONE=1;

while(GODONE);

INPUT2=(ADRESH*256)+ADRESL;

/***** PWM LIMIT *****/

if(INPUT1>410 && INPUT2>410)
{
    if(CCPR1L<45)
        CCPR1L=45;

    if(CCPR1L>85)
        CCPR1L=85;

    if(CCPR2L<45)
        CCPR2L=45;

    if(CCPR2L>85)
        CCPR2L=85;
}

```

```
/****** OUTPUT REGULATION******/
```

```
if(INPUT1>410 && INPUT2>410)
```

```
{
```

```
    delay1();
```

```
    if(REFF1>600)
```

```
        CCPR1L++;
```

```
    delay();
```

```
    if(REFF1<605)
```

```
        CCPR1L--;
```

```
    delay1();
```

```
    delay1();
```

```
    if(REFF2>600)
```

```
        CCPR2L++;
```

```
    delay();
```

```
    if(REFF2<605)
```

```
        CCPR2L--;
```

```
    delay1();
```

```
}
```

```
/******
```

```
if(INPUT1>700 && INPUT2>700)
```

```
    SW=1;
```

```
if(INPUT1<600)
```

```
{
```

```
    SW=0;
```



```

        if(INPUT1<400)
        {
            SW=0;
            CCPR1L=100;
        }
    }

    if(INPUT2<600)
    {
        SW=0;
        if(INPUT2<400)
        {
            SW=0;
            CCPR2L=100;
        }
    }
}

void interrupt isr()
{
    if(TMR1IF==1)
    {
        TMR1IF=0;
        TMR1L=0XF0;
        TMR1H=0XD8;
    }
}

```

```

        count++;
        if(count==1)
        {
            PORTB=0;

            S1=1;

            S2=1;

        }
        if(count==2)
        {
            count=0;

            PORTB=0;

            S3=1;

            S4=1;

        }
    }
}
delay()
{
    unsigned int i;
    for(i=0;i<100;i++);
}
delay1()
{
    unsigned int j;
    for(j=0;j<10000;j++); }

```